From the
Department of Medical Biochemistry and Biophysics
Karolinska Institutet, Stockholm, Sweden

MOLECULAR MECHANISMS OF AMYLOID SELF-REGULATION

Michael Landreh

Karolinska Institutet

Stockholm 2012

Published by Karolinska Institutet. Printed by ReproPrint AB, Solna

ISBN **978-91-7457-974-1**

“Weiss nix, kann aber alles erklären.” (Hanns Dieter Hüsch)

ABSTRACT

Amyloid is associated with both pathological protein deposits and the formation of functional protein structures. Therefore, several strategies have evolved to control the formation or inhibition of amyloid *in vivo*. In this thesis, three separate systems were investigated in which amyloidogenic protein segments are coupled to regulatory elements that prevent or promote fibrillation. We describe the molecular mechanism for how (a) a propeptide segment prevents the uncontrolled aggregation of the mature peptide, (b) a chaperone domain inhibits amyloid formation, and (c) a pH-dependent relay controls protein assembly. For this purpose, mass spectrometry (MS)-based approaches to structural biology were applied and extended, involving gas phase interaction studies and hydrogen/deuterium exchange MS.

(a) Proinsulin C-peptide is beneficial for the preservation of insulin activity. We show that C-peptide interferes with insulin amyloid fibril formation at low pH and how conserved glutamate residues in C-peptide mediate reversible co-precipitation with insulin. A mechanism is proposed for how the balance between zinc and C-peptide mediates sorting of insulin into slow acting and rapid acting forms inside the secretory granules of the pancreatic β-cells, which potentially links C-peptide to diabetes type 1 and 2.

(b) Lung surfactant protein C (SP-C) is a highly amyloidogenic transmembrane polypeptide that controls surface tension in the alveolar phospholipid bilayer. Its proprotein includes a conserved chaperone domain termed BRICHOS, which is also associated with neurodegenerative disorders. It is shown here how BRICHOS and its N-terminal linker recognize hydrophobic residues and trap the SP-C segment in a β-hairpin conformation to prevent amyloid formation.

(c) Spider silk is synthesized as a highly soluble protein that assembles into silk in a pH-dependent fashion. It is shown that the spider silk protein N-terminal (NT) domain dimerizes at the same pH interval that triggers silk assembly, and we define the associated structural changes. Furthermore, the use of the NT domain as a solubility tag for the expression of aggregation-prone proteins is demonstrated.

In summary, we have determined the molecular basis for three distinct mechanisms by which fibril formation is controlled through autoregulatory elements and provide insights into nature's strategies to control amyloid formation and prevention. Based on these findings, we can now make conclusions about nature's handling of amyloidogenic proteins and their function in general.

LIST OF PUBLICATIONS

This thesis is based on the following publications, which are referred to by their Roman numerals:

I. Nerelius, C., **Fitzen, M.,** Johansson, J. (2010) *Amino acid sequence determinants and molecular chaperones in amyloid fibril formation.* **Biochem. Biophys. Res. Commun. 396:** 2-6.

II. **Landreh, M.,** Astorga-Wells, J., Johansson, J., Bergman, T., Jörnvall, H. (2011) *New developments in protein structure and function analysis by mass spectrometry and use of H/D exchange microfluidics.* **FEBS J. 278:** 3815–3821.

III. Astorga-Wells, J.*****, **Landreh, M.*,** Bergman, T., Jörnvall, H. (2011) *A membrane cell for on-line Hydrogen/Deuterium exchange to study protein folding and protein-protein interaction by mass spectrometry.* **Mol. Cell. Proteomics 10:** M110.006510

IV. **Landreh, M.,** Stukenborg, J.-B., Willander, H., Söder, O., Johansson, J., Jörnvall, H. (2012) *Proinsulin C-peptide interferes with insulin fibril formation.* **Biochem. Biophys. Res. Commun. 418:** 489-93.

V. **Landreh, M.,** Alvelius, G., Willander, H., Stukenborg, J.-B., Söder, O., Johansson, J., Jörnvall, H. (2012) *Insulin solubility transitions by pH-dependent interactions with proinsulin C-peptide.* **FEBS J.** *In press.* **DOI:** 10.1111/febs.12045

VI. **Landreh, M.,** Johansson, J., Jörnvall, H. *Interactions of proinsulin C-peptide in the beta cell secretory granule: A molecular balance with implications for diabetes-associated conditions*. **Submitted.**

VII. **Fitzen, M.,** Alvelius, G., Nordling, K., Jörnvall, H., Bergman, T., Johansson, J. (2009) *Peptide-binding specificity of the prosurfactant protein C Brichos domain analyzed by electrospray ionization mass spectrometry.* **Rapid Commun. Mass Spectrom. 23:** 3591-8.

VIII. Willander, H.*****, Askarieh, G.*****, **Landreh, M.*,** Westermark, P., Nordling, K., Keränen, H., Hermansson, E., Hamvas, A., Nogee, L.M., Bergman, T., Saenz, A., Casals, C., Åqvist, J., Jörnvall, H., Berglund, H., Presto, J., Knight, S.D., Johansson, J. (2012) *High-resolution structure of an intramolecular chaperone. Implications for anti-amyloid activity of the BRICHOS domain.* **Proc. Natl. Acad. Sci. USA. 109:** 2325-9.

IX. Peng, S., **Fitzen, M.,** Jörnvall, H., Johansson, J. (2010). *The extracellular domain of Bri2 (ITM2B) binds the ABri peptide (1-23) and amyloid beta-peptide (Abeta1-40). Implications for Bri2 effects on processing of amyloid precursor protein and Abeta aggregation.* **Biochem. Biophys. Res. Commun. 393**: 356-61.

X. **Landreh, M.,** Askarieh, G., Nordling, K., Hedhammar, M., Rising, A., Astorga-Wells, J., Alvelius, G., Casals, C., Knight, S. D., Johansson, J., Jörnvall, H., and Bergman, T. (2010) *A pH-dependent dimer lock in spider silk protein*. **J. Mol. Biol. 404:** 328-36.

XI. Jaudzems, K., Askarieh, G., **Landreh, M.,** Nordling, K., Hedhammar, M., Jörnvall, H., Rising, A., Knight, S. D., and Johansson, J. (2012) *pH-dependent dimerization of spider silk N-terminal domain requires relocation of a wedged tryptophan side-chain*. **J. Mol. Biol. 422:** 477-87.

XII. Rising, A., Nordling, K, **Landreh, M.,** Lindqvist, A., Johansson, J. *The N-terminal domain of spider silk proteins as solubility-enhancing tag for recombinant protein production.* **Manuscript.**

XIII. **Landreh, M.,** Johansson, J., Rising, A., Presto, J., and Jörnvall, H. (2012) *Control of amyloid assembly by autoregulation*. **Biochem. J. 447:** 185-192.

*** equal contribution**

PUBLICATIONS NOT INCLUDED IN THIS THESIS

1. Blume, A.*****, **Fitzen, M.*,** Benie, A.J., Peters, T. (2009) *Specificity of ligand binding to yeast hexokinase PII studied by STD-NMR.* **Carbohydr. Res. 344**: 1567-74.

2. Yang, L., Johansson, J., Risdale, R., Willander, H., **Fitzen, M.,** Akinbi, H.T., Weaver, T.E. (2010). *Surfactant protein B propeptide contains a saposin-like protein domain with antimicrobial activity at low pH.* **J. Immunol. 184:** 975-83.

3. Nerelius, C., Lindahl, E., **Landreh, M.,** Jörnvall, H. (2011) *Peptide interactions of proinsulin C-peptide.* In: Diabetes and C-Peptide: Scientific and Clinical Aspects (Anders A. F. Sima, Ed.) Springer, NY. ***DOI:****10.1007/978-1-61779-391-2_2.*

4. Liu, N., **Landreh, M.**, Cao, K., Abe, M., Hendriks, J.-G., Kennerdell, J., Zhu, Y., Wang, L.S., Bonini, N.M. (2012) *The microRNA miR-34 modulates ageing and neurodegeneration in Drosophila.* **Nature. 482:** 519-23.

*** equal contribution**

CONTENTS

LIST OF ABBREVIATIONS

Aβ	Amyloid β peptide
AD	Alzheimer's Disease
ALS	Amyotrophic lateral sclerosis
Bis-ANS	4,4'-Bis(1-anilinonaphthalene 8-sulfonate)
CID	Collision-induced dissociation
CTC	C-terminus of proSP-C
ECD	Electron capture dissociation
EM	Electron microscopy
ESI-MS	Electrospray ionization mass spectrometry
FBD	Familial British dementia
FDD	Familial Danish dementia
HDX-MS	Hydrogen/deuterium exchange mass spectrometry
HSP	Heat shock protein
IAPP	Islet amyloid polypeptide
ILD	Interstitial lung disease
MS	Mass spectrometry
MaSp	Major ampullate silk fibroin protein
NT	N-terminal
OD_{500}	Optical density at 500 nm
PD	Parkinson's Disease
PolyQ	Polyglutamine
PrP	Prion protein
SP-C	Surfactant protein C
ThT	Thioflavin T
Trx	Thioredoxin
Wt	Wild type

1 PREFACE

This thesis summarizes research conducted over the years 2008 - 2012 at the Department of Medical Biochemistry and Biophysics (MBB), Karolinska Institutet (KI), a department devoted to the study of molecular mechanisms of human disease.

The work combines research on diabetes, neurodegenerative disease, and spider silk formation, with emphasis on application and development of mass spectrometrical methods in protein structure analysis for conclusions about amyloidogenic proteins in general. The thesis contains a wide spread of methods, structures, and diseases, which was made possible through the fruitful collaboration of my three supervisors, Professors Hans Jörnvall, Tomas Bergman, and Jan Johansson. As indicated by the author list for each paper included in this thesis, not all publications are based on my work primarily, but I was able to make significant contributions to each thanks to the versatility and robustness of mass spectrometry-based protein structure analysis. Accordingly, I have focused on my contributions to the publications, and only the corresponding methods are included in the Methodology section. However, I was always involved in discussions of key results and in the preparation of the final manuscripts, and have included all studies to provide a complete picture.

At the start of my Ph.D. studies, we designed a three-phase project: the first phase aimed to establish and extend Hydrogen/Deuterium Exchange (HDX) Mass Spectrometry (MS), the second phase to apply MS-based methods to investigate the chaperone activity of the BRICHOS domain on lung surfactant protein C (SP-C), and the third phase to broaden the HDX-MS-based investigations to include other amyloid-related proteins.

Phase one and two resulted in four publications (Paper III and Papers VII, VIII, and IX, respectively). However, already at the end of the first phase, the opportunity arose to apply MS to study the pH-dependent assembly of spider silk, which is under investigation in the group of Jan Johansson. My involvement resulted in an MS-based publication (Paper X) and allowed me to contribute mass spectrometrical analyses during the follow-up investigations (Papers XI and XII). Since Hans Jörnvall has a long-standing interest in the biological role of proinsulin C-peptide and its chaperone-like effect on mature insulin, he suggested to further broaden the scope of this work to clarify the nature of this interaction. Our findings and the resulting implications are summarized in Papers IV, V, and VI.

During the course of my studies, it became obvious that the ability to regulate amyloid formation is a common feature of these three protein systems, either in its prevention, as exemplified by insulin and SP-C biogenesis, or its controlled occurrence, as in spider silk assembly. C-peptide, the BRICHOS domain, and the spidroin N-terminal domain all represent controlling elements in the (pro)protein and act as an intrinsic modulator of amyloid formation. This primed us to search the literature for more examples of self-regulating amyloid. We have summarized the well-characterized systems in an article that places the results presented in this thesis in the context of the current state of amyloid research and concludes this thesis (Paper XIII).

Furthermore, I have chosen to include two overview articles as an introduction: a summary of the nature of amyloid and its prevention (Paper I) and a description of mass spectrometry as a protein structure analysis tool (Paper II).

2 INTRODUCTION

2.1 STRUCTURAL FEATURES OF AMYLOID (PAPER I)

2.1.1 What is amyloid?

A long-standing dogma of molecular biology has stated that for each polypeptide chain, a specific conformation exists that defines its lowest energy structure and represents its native state. The universal validity of this hypothesis, however, has been challenged by a discovery that precedes it by more than 300 years.

In 1639, the Italian physician Nicolaus Fontanus reported a wax-like abnormality in the spleen of a patient with liver failure. In 1854, Rudolf Virchow introduced the term “amyloid” for its macroscopic resemblance to an amylaceous (i.e. starchy) plant constituent, but noted that “only when we have discovered the means of isolating the amyloid substance shall we be able to come to any definite conclusion with regard to its nature” [1].

While reports of similar pathological abnormalities were subsequently linked to a variety of diseases, it was not until 1859 that protein was suggested to be constituent and, in 1931, was identified as the primary component of amyloid. Since then, advances in the use of chemical dyes, electron microscopy (EM) and, finally, high resolution protein structure analysis have led to the realization that amyloid represents a distinct class of (mis)folded proteins [2].

The modern biophysical definition states that proteins in the amyloid state exhibit green fluorescence when stained with Thioflavin T (ThT), as well as green birefringence when stained with Congo Red and viewed under polarized light. In EM, amyloid appears as straight, unbranched fibers with diameters between 6 and 12 nm. X-ray diffraction shows a pattern characteristic for β-sheets that run perpendicular to the fibril axis. The β-sheet motif is repeated periodically by thousands and thousands of stacked subunits that are usually composed of a single peptide each (Figure 1) [3]. Structural characteristics as well as strategies to prevent amyloid formation, outlined below, are discussed in Paper I.

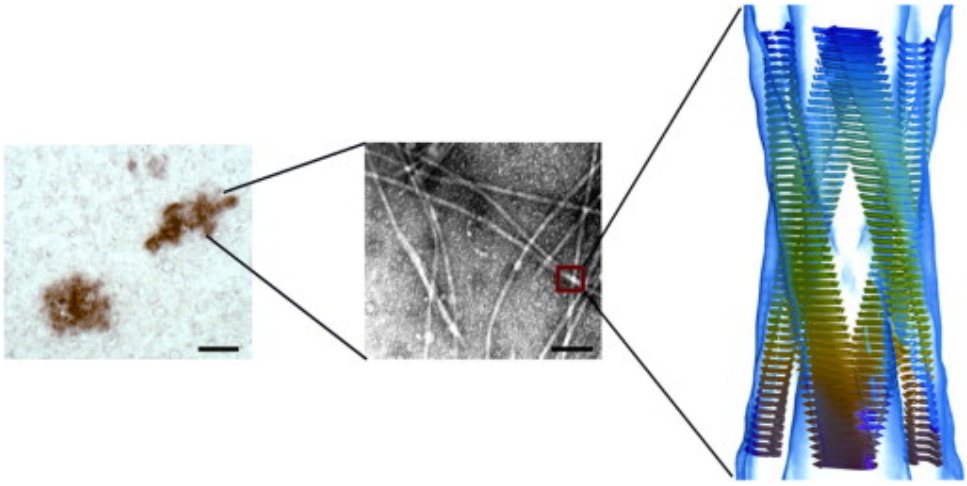

Figure 1. Structural organization of pathogenic amyloid. Amyloid plaques as observed in the brain of AD patients (left panel) are composed of individual fibrils, as visualized by EM (middle panel). The molecular structure of such fibrils consists of regularly stacked β-sheets from multiple copies of a single protein or peptide species (right panel). Scale bars represent 50 μM in the plaque and 100 nm in the EM micrograph. Reproduced from Paper I.

2.1.2 Molecular structure and sequence determinants of amyloid fibrils

Even though amyloid fibrils possess such a highly ordered nature, insights into their molecular structure are notoriously difficult to obtain, and to date a solid-state NMR structure [4] as well as a small variety of crystal structures of nanofibers and 3D-crystals [5] exist.

While it has long been a matter of discussion whether the ability to form amyloid fibrils is a general property of the protein backbone, only a minor subset of proteins can form amyloid *in vivo.* This means that some proteins contain unprotected amyloid formation "hotspots" in their sequence that allows amyloid formation under physiological conditions [6]. On the other hand, the ability to form amyloid fibrils is a general feature but controlled to occur only under very specific circumstances, such as presence at high concentrations, altered pH, and together with destabilizing agents [7].

The suggestion that some sequences are more prone to aggregation than others is supported by studies on fragments of amyloid disease-associated proteins. Amyloid-forming sequence motifs have been found *e.g.* in insulin, the Alzheimer's Disease (AD)-related Amyloid β peptide (Aβ), the yeast Sup35 prion, prion protein, and islet amyloid polypeptide. Crystal structures derived from such short model peptides exhibit the expected parallel or antiparallel β-strand register. Surprisingly, some of the short model peptides have been found to form very densely packed "steric zipper" structures, in which sidechains and backbone amides form a tight interaction that excludes water from the interface [5, 8, 9].

However, no obvious sequence homology can be derived from these motifs, and amyloid peptide structures have been reported that do not feature steric zipper motifs [10]. Some structures contain tight interactions between aromatic sidechains instead, which have been suggested to mediate amyloid peptide assembly through stacking of π-bonds [11, 12]. While several model peptides contain aromatic residues, it has been demonstrated that they can be replaced by non-aromatic, hydrophobic amino acids without losing the ability to form amyloid fibrils, as long as a balance of negative and positive sidechains is maintained [13].

Several prediction strategies have been described to identify amyloid-forming sequences, based on their content of β-sheet stabilizing or de-stabilizing residues [14, 15], the ability of the sidechains to pack into a β-sheet structure [16], or by assignment of an "aggregation score" for each amino acid based on its occurrence in α-helices and β-sheets, hydrophobicity, and charge [17].

A different approach is the identification of stretches in amyloid-forming proteins that form α-helices but have a higher propensity to form β-sheets [18]. A prominent example of such a "frustrated" or discordant helix is the lung surfactant protein C (SP-C), the mature form of which contains a 12-residue poly-valine stretch that forms a transmembrane helix when inserted into the lung surfactant phospholipid bilayer [19], but is thermodynamically unstable and forms β-sheet aggregates *in vitro* [20].

A "reverse" example of sequence discordance in β-sheet conversion is the aggregation of arthropod major ampullate silk proteins (MaSp), the main constituents of spider dragline silk (see section **2.5**). MaSp are mostly unstructured or helical in solution [21] and have a high α-helix propensity, but form β-sheet crystalline blocks during silk assembly [22, 23] and give the assembled spider silk amyloid fibril-like properties [24].

2.1.3 Mutations, miscleavages, transmission: Pathogenic amyloid

Most amyloid deposits formed *in vivo* are disease-associated. As of 2012, 28 proteins have been described to form amyloid fibrils that are linked to human disease and can occur either as accompanying symptom or molecular cause of the disease [25]. The reasons for conversion of a folded protein into amyloid fibrils are only partially known and include mutations, cleavage, and interactions with other misfolded proteins.

Mutations can cause the generation of amyloidogenic species, as in the familial Danish and British Dementias (FDD and FBD), where a stop-codon mutation extends the 23-residue C-terminal signal peptide of the Bri2 gene product to 34 residues and strongly increases its aggregation propensity [26, 27].

(Mis)Cleavage of precursor peptides can also generate amyloid-forming products, as exemplified by the amyloid β precursor protein (APP), which gives rise to $A\beta_{1-40}$ and $A\beta_{1-42}$ as well as the less toxic $A\beta_{1-39}$ peptides. Formation of the toxic $A\beta_{1-42}$ oligomers and subsequent aggregation into amyloid fibrils are thought to be responsible for AD.

A special case is the self-propagating misfolding mechanism that is observed in spongiform encephalopathies caused by aggregated prion protein (PrP^{SC}). Here, a small fraction of misfolded PrP can trigger conversion of the folded cellular PrP^{C} into the pathogenic, amyloid-forming PrP^{SC} form, which makes PrP^{SC} an infectious agent [28]. Interestingly, similar behavior has recently been reported for the Aβ peptide, which, when injected in amyloid form, can induce β-amyloidosis in mice [29]. Several additional factors have been described to influence amyloid formation *in vivo*, such as protein concentration, *e.g.* in localized insulin amyloidosis in diabetic patients, where high local insulin concentrations at the site of repeated injections give rise to amyloid deposits composed of misfolded insulin [30]. Similarly, post-translational modifications, *e.g.* in neurofibrillar tangles formed by hyperphosphorylated tau protein, are thought to contribute to AD [31]. Most proteins associated with protein aggregation diseases have been found to form amyloid fibrils also *in vitro*, such as mutant ataxins (Polyglutamine diseases, PolyQ) [32] and α-synuclein (Parkinson's Disease, PD) [33]. In these cases, *in vivo* occurrence of plaques with amyloid properties might have escaped detection, or do not share all known characteristics of amyloid deposits [25].

2.2 CONTROL OF AMYLOID FORMATION IN VIVO

2.2.1 Molecular chaperones in protein aggregation diseases

Common to most amyloid-forming proteins is the existence of aggregation-prone sequence elements. Hence, stabilization of such motifs by molecular chaperones represents a possible approach to the prevention of amyloid formation.

Two approaches have successfully demonstrated the relation between molecular chaperones and protein aggregation diseases: Expression of molecular chaperones in protein aggregation disease models, and proteomics- and immunohistochemistry-based characterization of the content of protein aggregates isolated from patient material.

Both approaches have identified chaperones of the heat shock protein (HSP) families as potential modulators of protein aggregation. In the case of co-expression of molecular chaperones with protein aggregation disease-related genes, it was found

that HSP70 rescues cultured neurons expressing $A\beta_{1-42}$ by reducing aggregate load [34], and similarly promotes α-synuclein refolding in a cell culture model of PD [35]. Neuroprotective effects of HSPs have been demonstrated in *Drosophila* PD [36] and PolyQ disease [37, 38] models. Subsequently, an HSP-related pathway was identified as component of Aβ proteostasis in a *C.elegans* model of AD [39]. Pharmacological induction of HSP expression has also been shown to delay the progression of amyotrophic lateral sclerosis (ALS) in a mouse model [40]. Furthermore, analyses of patient-derived protein deposits have confirmed the presence of HSPs in aggregates from AD, PD, HD, PolyQ diseases, Lewy Body dementia, and ALS (summarized in [41]). This suggests that molecular chaperones can be effectively used to combat pathogenic protein aggregation.

However, since the latter examples lack the biochemical hallmarks of amyloid disease [25], the only reported instance of chaperone activity against established pathogenic amyloid is the connection between HSPs and Aβ aggregation in AD, and to date no case of *in vivo* amyloid formation due to malfunction of a non-specific chaperone has been described.

2.2.2 The emerging concept of functional amyloid

While amyloid formation is predominantly seen as a hallmark of protein aggregation disease, a growing body of evidence suggests that certain forms of amyloid can serve specific biological functions. The first “functional amyloids”, as they were termed, were reported to form fimbriae of gram-negative *E. coli* [42]. These fimbriae, which serve in bacterial surface adhesion, are composed of six proteins of the Csg family and share features of amyloid fibrils such as morphological similarity and ThT and Congo Red stainability [43]. A second bacterial amyloid, but with a different biological function, was detected to be the Chaplin proteins that aid spore dispersal [44]. Subsequently, several additional bacterial amyloids with roles in biofilm formation, surface attachment, and pore formation were described (reviewed in [45]).

The first eukaryotic example was the yeast Sup35 prion: In soluble form, it serves as DNA transcription factor, while its ability to assemble into amyloid fibrils allows its transmission (in active or inactive form) to the next generation as a non-genetic element of inheritance [46].

In recent years, two reports have described functional amyloid in humans: melanin biosynthesis was found to require amyloid fibril formation by the Pmel17 protein. Pmel17 amyloid functions as scaffold for the assembly of melanin polymers while

preventing the release of toxic melanin precursors [47]. Furthermore, it was reported that 31 different human peptide hormones were capable of forming non-toxic amyloid assemblies in secretory granules but can be released in biologically active form [48].
Another type of protein assembly with amyloid-like properties is the family of arthropod silks, *i.e.* spider silk. Of the different spider silks that fulfill diverse functions and possess a variety of chemical and physical properties, the spider dragline silk is the most studied. Assembly of the aggregation-prone regions of MaSp1 (that represent the main constituent of dragline silk) in the duct of the spider silk glands converts the soluble “storage” form into the β-sheet silk form [23].

2.2.3 Regulatory strategies to control amyloid formation

Due to the extreme stability and potentially toxic nature of amyloid, the apparently beneficial presence of amyloidogenic proteins and peptides requires sophisticated control mechanisms that go beyond those provided by most molecular chaperones. Three basic strategies have evolved to regulate the formation of functional amyloid:
(1) **Specialized chaperones** regulate the assembly of prions into amyloid fibrils in yeast. The chaperone HSP104 represents one of few known examples for specialized amyloid chaperoning systems and is unique in its ability to disassemble amyloid fibers composed of the yeast prion protein Sup35 [49]. Proinsulin C-peptide can be considered an example of a chaperoning domain as it blocks the conversion of insulin into amyloid fibrils (see section **2.3**). Another example is the proSP-C BRICHOS domain, which has a chaperoning function that prevents the formation of pathogenic amyloid, but is also an auto-regulatory element (see section **2.4**).
(2) **Regulatory domains** have been identified in functional amyloids, such as the yeast HET-s and HET-S prions, as well as in the proteins that form spider silk. Here, conformational changes in “switch domains” trigger or prevent aggregation. Spider silk spidroins contain N- and C-terminal non-repetitive domains, which control fiber assembly by responding to pulling forces during spinning as well as changes in salt concentration and pH along the spinning duct ([50] and section **2.5**).
(3) **Selective precursor processing** has been suggested to play a major role in the assembly of functional amyloids such as the assembly of peptide hormone amyloid, where cleavage of proforms is thought to generate more or less amyloidogenic species [48]. C-peptide still affects insulin amyloid formation after excision from proinsulin during insulin processing (see section **2.3**) and thus provides evidence that selective processing of blocking elements can be used to control amyloid formation *in vivo*.

2.3 PROINSULIN PROCESSING AND AMYLOID FORMATION

2.3.1 Insulin biogenesis and processing

Insulin is a 51-residue peptide hormone that promotes glucose uptake. Type-I diabetes is caused by insulin deficiency which can be treated by administration of recombinant insulin through subcutaneous injection. The mature form is composed of two mostly helical polypeptide chains linked by two inter- and a single intramolecular disulfide bridge [51]. Its precursor proinsulin is produced in the islets of Langerhans [52]. Subsequent cleavage by type-I and –II endopeptidases releases mature insulin and the 31-residue C-peptide, which is co-secreted with insulin into the blood stream and has a variety of molecular actions [53-55]. C-peptide is largely unstructured in solution except for a potential β-turn motif at the C-terminus [56] and can form large oligomers under physiological conditions [57]. C-peptide is required for correct folding of proinsulin [58, 59], which is dependent on the N-terminal acidic residues Glu3, Glu5, and Asp6 [60]. Additionally, co-administration of insulin and C-peptide in diabetic rats accelerated insulin uptake [61], suggesting that C-peptide has a chaperone-like activity towards insulin [62].

2.3.2 Regulation of insulin amyloid fibril formation

At low pH, high concentrations, and elevated temperature, native insulin can assemble into amyloid-like fibrils, in which the insulin monomers adopt a cross-β-sheet structure. Using mass spectrometry, insulin has been shown to form soluble multimers at low pH that are composed of 2, 3, 6 or 12 monomers. These multimers are in rapid equilibrium with the monomeric form and increase with increasing insulin concentration [63], but retain essentially the same structure as native insulin [64]. However, longer exposure to these conditions causes partial unfolding of the monomer [65, 66] and subsequent assembly into amyloid-like fibrils composed of 2, 4, and 6 protofilaments [67].

Insulin-containing amyloid deposits have been observed in patients with type-I diabetes [30]. In these cases, cutaneous local amyloidosis occurs at the site of repeated insulin injection in patients using human recombinant and/or porcine insulin [68, 69]. Formation of these aggregates is attributed to the high local insulin concentrations as well as the increased aggregation propensity of the faster-acting, mostly monomeric “LisPro” insulin variant [70].

In order to prevent insulin aggregation and increase bioavailability of the hormone, several strategies for inhibition of fibril formation have been tested, including amino sugars [71], soluble insulin A and B-chains [72], presence of hydrophilic surfaces and solvents [73], small aromatic molecules [74], molecules associated with stress reactions [75], and engineered peptides derived from the insulin B-chain [76]. With the exception of native A- and B-chain, all of these inhibitors were ineffective unless used in >4-fold excess over insulin.

Interestingly, it has been reported that proinsulin is refractory to insulin fibrillation. While it can form β-sheet-rich aggregates under the same conditions as mature insulin, they remain morphologically different from insulin fibrils and exhibit significantly extended aggregation lag times. It was concluded that proinsulin aggregation is hindered by the covalent linkage of insulin A- and B-chain, posing a conformational restraint by connecting the N- and C-termini of the insulin polypeptide chains that prevents the structural re-arrangement into a cross-β-sheet structure. We hypothesize that the absence of insulin amyloid from secretory granules, despite the high local concentrations, could also be due to post-cleavage C-peptide effects.

2.4 BRICHOS DOMAINS AND THEIR ROLES IN PROTEIN AGGREGATION DISEASES

2.4.1 BRICHOS-containing proteins

The BRICHOS domain was first identified by Sanchez-Pulido *et al.* in 2002 [77] from multiple sequence alignments. Three families of BRICHOS-containing proteins were described: The Bri genes 1-3 (also referred to as ITM2A-C), one homologue of which causes familial *Bri*tish dementia [27], Mature *Cho*ndromodulin-I, associated with chondrosarkoma [78], and the proform of lung *s*urfactant protein C. In a recent investigation, more than 300 different proteins in 12 families were found to contain BRICHOS domains [79]. The architecture of these proteins is surprisingly similar. Common to all is the presence of an N-terminal hydrophobic region that is predicted to be helical, a linker region that is predicted to be coiled or helical, the actual BRICHOS domain, and a C-terminal segment (Figure 2). Overall sequence conservation is low, with only three residues conserved among all BRICHOS domains: D105, C120 and C188 (numbering according to human proSP-C). In human proSP-C BRICHOS, the cysteines form an intramolecular disulfide bond [80]. Secondary structure predictions of all BRICHOS domains suggest that they share a common fold [79].

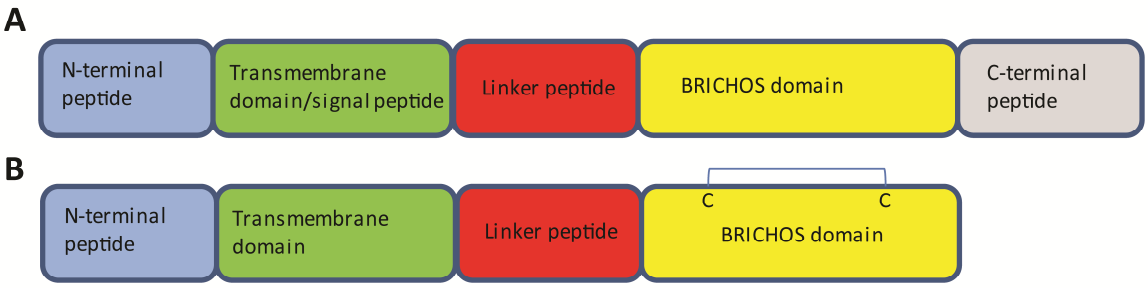

Figure 2. Organization of BRICHOS-containing proteins. BRICHOS-containing proteins are characterized by a transmembrane (TM) segment with an N-terminal signaling peptide, a linker region, and the BRICHOS domain. (A) Most BRICHOS-containing proteins feature a C-terminal segment not found in proSP-C which is predicted to form β-strands [81]. (B) In case of proSP-C, two strictly conserved cysteines form an intramolecular disulfide bond, and the transmembrane region has high β-strand propensity.

2.4.2 Biological and structural features of proSP-C

The transmembrane segment of the proSP-C protein is the lung *S*urfactant *P*rotein *C*. SP-C lowers the surface tension at the surfactant's air-water interface and prevents collapse of the alveoli during end expiration. Mature SP-C has 35 residues with a stretch of 12 valine residues that forms the transmembrane helix (see section **1.2.2**). SP-C is released by enzymatic cleavage from a 197-residue proform, which, besides the mature SP-C sequence, contains the already described linker and a BRICHOS domain on the C-terminal side in the endoplasmic reticulum.

A clue to the function of proSP-C BRICHOS came from the observation that mutations in the proSP-C gene *SFTPC* have been identified as the cause of interstitial lung disease (ILD). Intracellular protein aggregates composed of SP-C were found in the alveolar type II epithelial cells normally expressing proSP-C for secretion [82]. To date, over 50 *SFTPC* mutations have been described. Interestingly, while most mutations that give rise to protein aggregation in other systems are located within the aggregating protein itself, the majority of the *SFTPC* mutations that cause SP-C aggregation are not located in the region that comprises mature SP-C, but in the linker and BRICHOS domains [83, 84]. Expression of mature SP-C without its linker and BRICHOS segments results in virtually undetectable expression levels, but expression in soluble form can be elevated by co-expression with the linker and BRICHOS (a construct further referred to as CTC, *i.e.* "C-terminus of proSP-C") on a separate vector [85]. In line with this observation, purified recombinant CTC was found to prevent aggregation of peptides with discordant helices prone to amyloid formation, such as polyvaline and

the $A\beta_{1-40}$ peptide, while the mutations that are linked to ILD were found to interfere with its anti-amyloid activity [82]. Additionally, binding of purified recombinant CTC to decamers composed of a single amino acid covalently linked to cellulose membranes showed that CTC can interact with hydrophobic residues that have a high β-sheet propensity [86]. In paper VII, we have conducted a mass spectrometric investigation of CTC and BRICHOS ligand preferences using gas phase binding to acquire gas phase K_Ds, and CID were used to measure of relative complex stability.

Using limited proteolysis, it could be shown that the BRICHOS domain is highly resistant to tryptic digestion and stabilized by two intramolecular disulfide bonds. Binding of the hydrophobic dye 4,4'-Bis(1-anilinonaphthalene 8-sulfonate) (Bis-ANS) suggests that a major fraction of the five tyrosines in CTC are located in a hydrophobic environment, which could represent a binding site for hydrophobic target peptides [80]. In paper VIII, we present the crystal structure of the protease-resistant core of BRICHOS as well as the identification of a putative binding site involving the BRICHOS domain and the linker region as interaction partners of a polyvaline ligand. We report the observation of amyloid deposits in patients with *SFTPC* mutations in the linker and BRICHOS regions, which suggests that aberrant chaperone function can give rise to amyloid disease *in vivo.*

2.4.3 Bri2 and its related familial dementias

Interestingly, other BRICHOS-containing proteins besides proSP-C are associated with protein aggregation disease. Vidal *et al.* reported amyloid deposits in the brain of patients with FDD and FBD [26, 27] which were composed of an extended C-terminal peptide from the Bri2 protein that is expressed in several tissues of the brain, but most prominently in neurons of the hippocampus and the cerebellum [87]. The wt peptide, Bri23, is 23 residues long and, like the 32-residue mutant form (ABri) that is released from Bri2 by furin cleavage [88]. Several studies have pointed towards a relationship between APP processing and Bri2: Aβ accumulation was found to be inhibited through binding of Bri2 to APP [89], and their interaction to be mediated by their respective transmembrane domains. Subsequent *in vivo* studies in a mouse model of AD revealed that Bri2 inhibits Aβ accumulation [90]. The link between Bri2 and AD was further supported by the observation that amyloid plaques from FDD patients contain Aβ peptide, suggesting that ABri32 aggregation occurs in interaction with Aβ [81] and is promoted by increased APP processing [91]. Interestingly, the Bri23 peptide can inhibit Aβ aggregation *in vitro* and *in vivo* [90, 92]. Secondary structure predictions of Bri2

indicate a preference for β-sheet conformation in the Bri23 peptide [81], which is analogous to the high β-sheet propensity of the transmembrane segment in proSP-C. In Paper IX, we present evidence that the Bri2 BRICHOS domain can also interact with peptides that have high β-sheet propensity (with Bri23 as the natural target) and prevent amyloid formation in a manner similar to the action of CTC.

2.5 SPIDER SILK AS AN AMYLOID-LIKE BIOMATERIAL

2.5.1 Spider silk assembly and structure

Spider silk is a proteinaceous biomaterial that has evolved to suit a wide variety of functions. Besides their superficial morphological similarity, the assembled fiber shares a number of characteristics with amyloid fibrils: assembled fibrils can be stained with ThT and Congo Red, their secondary structure has been calculated to contain more than 70% β-sheet and β-turn motifs, and show X-ray diffraction that indicate a β-sheet structure with close inter-sheet packing [24]. Solid-state NMR H/D exchange measurements, however, indicate that 50% of the alanine residues which are enriched in the repetitive domains of spider silk fibroins (see below) are accessible to water [93], indicating that assembled fibers are not completely composed of β-sheets, but contain significant amounts of unstructured regions. Molecular mechanics simulations have suggested that a balance between semi-extended coil regions and crystalline blocks composed of β-sheets could be responsible for the toughness and elasticity of the fiber (Figure 3) [94]. This illustrates that the unique mechanical properties of spider silk are achieved by controlled assembly of spidroins to contain tough, amyloid-like and elastic, disordered segments.

The most studied variant is dragline silk, which is mainly composed of major ampullate spidroin proteins 1 (MaSP1) and 2. They are stored in the major ampullate gland in the spider abdomen as a concentrated dope with a protein content of up to 50% (w/v) [95]. Interestingly, the proteins maintain a largely α-helical conformation even under these extreme conditions [21]. Silk assembly is initiated by pulling of the dope from the major ampullate gland's duct, which simultaneously (a) shifts the pH of the solution from approximately 7.0 to below 6.4 [96], (b) reduces the salt content of the dope [97], and (c) subjects the dope to pulling forces as it exits the duct [98].

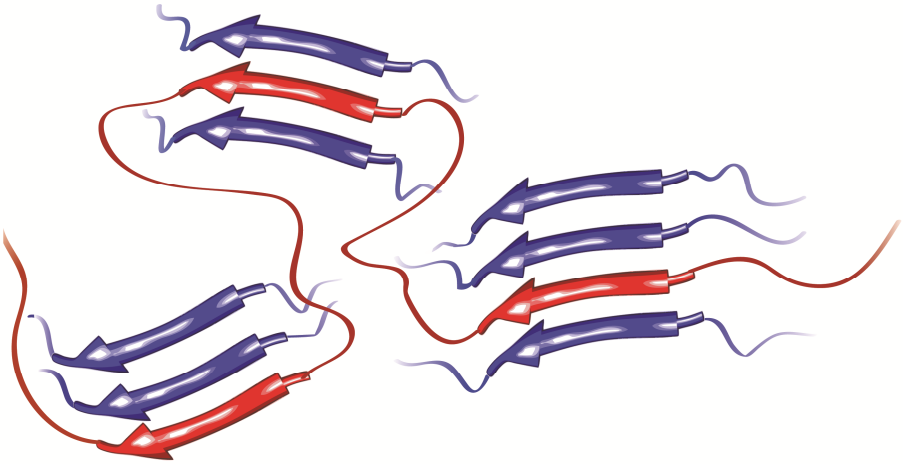

Figure 3. Proposed model of spider silk architecture. Assembled spider silk is composed of both β-sheet-rich and disordered, extended segments, indicating a balance between amyloid-like and flexible regions. A single fibroin chain is shown in red. Adapted from Paper XIII.

2.5.2 Architecture of MaSp proteins

The assembly of silk spidroins into fibers requires a unique arrangement of sequence motifs. MaSp proteins have a tripartite organization, with a non-repetitive, conserved N-terminal domain of ~130 amino acids, a long repetitive region composed of up to 3300 residues that contains alternating alanine- and glycine-rich segments, and a non-repetitive, conserved C-terminal domain of ~110 amino acids [99]. The alanine-rich segments have been assigned to β-sheet blocks, while specific glycine-containing motifs are predominantly found in 3_{10}-helices and β-spirals, the occurrence of which determines specific mechanical properties of the assembled silk [100].

It should be noted that neither glycine nor alanine-rich sequences can be regarded as amyloidogenic. Alanine is the amino acid with the highest α-helix propensity and therefore likely responsible for the high helix content of the spidroin protein dope. Yet, assembly of spider silk fibers converts the highly soluble spidroins to an amyloid-like material with β-sheet structure. Studies using truncated spidroin constructs have shown that the non-repetitive C-terminal domain is essential for fiber formation [101, 102] and can form macroscopic fibers on its own [103]. The high-resolution structure of the soluble C-terminal fragment supports the hypothesis that amphipathic helices in the entirely helical domain can refold to expose hydrophobic parts that in turn promote silk assembly. The C-terminal domain forms a disulfide-linked parallel dimer that has been proposed to align the repetitive elements during assembly [104].

The N-terminal (NT) non-repetitive domain, on the other hand, despite being the most conserved segment of the MaSp proteins, is not required for MaSp1 fiber formation *in*

vitro and has no known homologues in silk-forming proteins from other organisms [105]. However, its inclusion in recombinant spidroins promotes their assembly into fibrils at pH 6.3, while inhibiting their assembly at high salt concentrations [50]. This suggests that the NT domain acts as a molecular switch that senses the pH and salt concentration changes during extrusion from the duct and accelerates silk assembly accordingly. Its high-resolution crystal structure shows an antiparallel, non-covalent dimer of dipolar subunits, each composed of a 5-helix bundle. Replacement of conserved residues aspartate 40 (D40) and glutamate 84 (E84) interferes with the pH-dependent action of the NT domain, further supporting the suggestion that its function is charge-dependent [50]. However, how these charge interactions mediate silk assembly could not be determined from the crystal structure.

3 AIM OF THE THESIS

The aim of this thesis has been to investigate the self-regulatory strategies behind the control of amyloid formation in three protein systems: proinsulin processing, the biosynthesis of lung surfactant peptide C, and the assembly of spider silk. In order to study these mechanisms, we applied mainly gas phase interaction studies and H/D exchange mass spectrometry.

Specifically, we aimed to understand the molecular mechanisms by which

- proinsulin C-peptide chaperones insulin,
- the proSP-C BRICHOS domain stabilizes the highly amyloidogenic SP-C transmembrane segment, and
- the N-terminal domain of MaSp1 mediates the pH-dependent assembly of spider silk.

4 METHODOLOGY

4.1 MASS SPECTROMETRY IN PROTEIN STRUCTURE ANALYSIS (PAPER II)

4.1.1 Why mass spectrometry?

Since most amyloid-related proteins and peptides are refractory to standard protein analysis methods, mass spectrometry can be applied as an alternative for the investigation of their structure and function. Two principal strategies were employed: gas phase interaction analysis to monitor the formation of non-covalent complexes, and hydrogen/deuterium exchange mass spectrometry (HDX-MS) to monitor protein structural dynamics in solution. The background to both approaches is summarized in Paper II and briefly outlined below.

4.1.2 Protein structure in the gas phase

The development of electrospray ionization mass spectrometry (ESI-MS) provided soft ionization as a means to study intact protein molecules by mass spectrometry . Drops from a protein solution are then ionized and evaporated, leaving a charged protein species without solvent that is transferred into the vacuum chamber of a quadrupole time-of-flight mass spectrometer. In 1991, it was reported that ESI-MS could not only produce charged protein species but could also be used to transfer intact protein complexes into the gas phase [106]. Over time, evidence has accumulated that it is possible for proteins to retain their native fold even after desolvation. Longer exposure times to a solvent-free environment significantly alters protein structure, weakening hydrophobic while strengthening electrostatic interactions (reviewed in [107]). However, analysis of the electron capture dissociation (ECD) fragmentation pattern of a protein in an ion trap showed that salt bridges, secondary structure and hydrogen bonds were preserved for >4 seconds in vacuum [108].

These observations suggest that correctly folded protein species and intact protein complexes with a near-native fold can be studied by ESI-MS. Since the 1990s, several approaches have been developed, and the ensuing systematic studies found gas phase interactions to be partially comparable to solution-phase interactions (reviewed in [109]). The two most widely used applications that emerged were the determination of gas phase K_D values by direct titration, and the comparison of relative complex stabilities by collision-induced dissociation (CID) [110].

We have employed both strategies to investigate the substrate requirements for the chaperoning effect of the proSP-C BRICHOS domain (Paper VII). Homo-tripeptides were used to mimic peptide sequences with specific properties such as hydrophilic, hydrophobic, and aromatic segments. The determined ligand preferences correlate well with solution phase results (see section **5.1**), indicating that this approach can be successfully applied to the study of hydrophobic complexes.

A powerful proof of the possibility to observe even complex protein assemblies intact in the gas phase was provided by ion mobility mass spectrometry analysis of macromolecular ring-shaped assemblies of the trp RNA-binding protein. The resulting data provides compelling evidence for collapse of these rings in the absence of RNA molecules, while their presence was found to stabilize the ring structure [111].

4.1.3 H/D exchange mass spectrometry

The principle of H/D exchange was demonstrated by Linderstrøm-Lang as early as in the 1950s [112]. The speed of exchange of protein backbone amide hydrogens for deuterium depends on solvent accessibility and local secondary structure elements and can be accelerated or quenched by changes in pH and temperature [113, 114].

In 1991, the possibility to measure the exact amount of deuterium incorporation by mass spectrometry and its application in the determination of protein folding states was demonstrated [115]. The combination of enzymatic digestion of labeled protein, separation of the resulting peptides by liquid chromatography, and subsequent mass spectrometric quantification of the deuterium incorporation in each fragment can be used to identify slow and fast exchanging protein segments and yield information about the local protein backbone conformation [116].

Most notably, the application of HDX-MS is limited only by the efficiency of the enzymatic digestion and the resolution power of the chromatographic peptide separation. In recent years, this method was therefore used to investigate the structure of proteins that have eluded most conventional NMR and X-ray crystallography methods, such as the β-sheet core of Aβ 1-40 [117, 118], prion [119], and insulin [67] fibrils. *E.g.,* HDX-MS was successfully utilized to show that *in vivo* prion aggregates have structural features not found in amyloid fibrils generated from recombinant prions, which demonstrates the importance of the method [120].

We used HDX-MS to obtain information about unstructured segments of proSP-C BRICHOS that could not be visualized by X-ray crystallography to locate the ligand binding segment in the proSP-C linker region (Paper VIII). We also applied HDX-MS to

monitor structural dynamics of the N-terminus of MaSp1 and demonstrated that the pH-dependent assembly of spider silk is mediated by dimerization and structural tightening of the N-terminal domain (Paper X). Both studies illustrate how HDX-MS can complement crystallographic protein structure data with information about protein regions that could otherwise not be analyzed.

As described below, we also developed an automatable on-line HDX-MS system for dilution-free protein labeling and demonstrate its application by monitoring conformational changes in proteins (Paper III).

4.2 H/D EXCHANGE MICROFLUIDICS FOR PROTEIN STRUCTURE ANALYSIS (PAPER III)

4.2.1 Problems with conventional H/D exchange strategies

HDX-MS relies on the dilution of a protein stock solution in a deuterated buffer with a final D-content preferably above 80%. This ensures a one-directional exchange of the protein backbone hydrogens for deuterium. At fixed time points, the exchange is quenched and the incorporation of deuterium into individual protein segments is measured by MS.

This approach has two disadvantages: Firstly, the dilution of a protein stock solution in deuterated buffer by a factor of > 5x can only be achieved through the use of concentrated protein stock solutions, usually in the high µM or even mM range, which requires large amounts of material and can cause unwanted aggregation. Secondly, sample preparation involves multiple pipetting steps, which represents an additional error source. Hence, a dilution-free, automatable procedure is desirable.

4.2.2 Deuterium delivery via a membrane flow cell

To overcome these problems, deuterium delivery using a flow cell (HDX cell) with two channels separated by an ion-selective membrane was tested (Figure 4). One flow channel carries the sample (main channel), the other deuterium oxide (second channel). By adjusting the flow rate of the sample, the deuterium incorporation can be adjusted, while the flow of the D_2O determines the deuterium concentration in both channels. The cell can be coupled directly to the ESI inlet of a mass spectrometer or to an HPLC system that includes peptic digestion and reverse-phase separation prior to MS analysis.

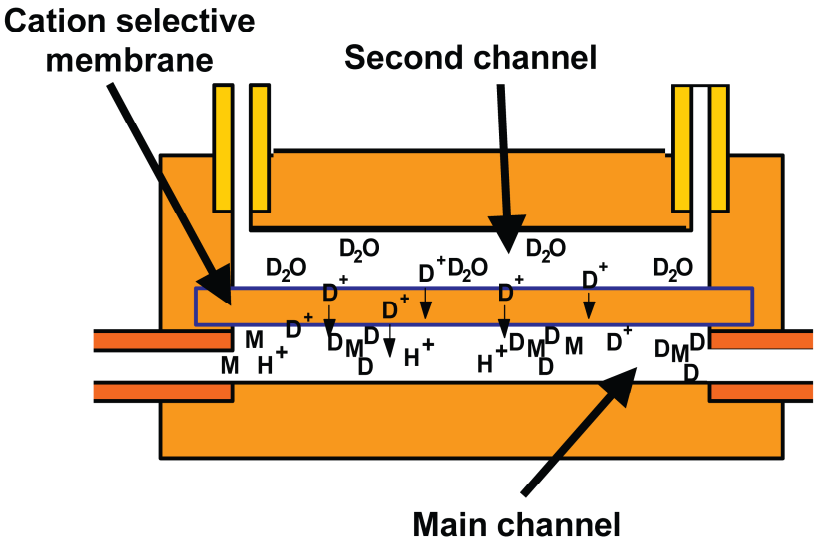

Figure 4. Layout of the HDX cell. The upper channel carries D_2O and is separated from the sample channel by a cation-selective membrane. D^+ and H^+ ions are freely transferred between the channels, allowing for deuterium labeling of protein transported in the sample channel. Reproduced from Paper III.

4.2.3 Method validation

To determine the amount of labeling afforded by the HDX cell, we measured the on-line deuteration of the unstructured [Glu1]-fibrinopeptide B at varying D_2O flow rates and compared it to the off-line deuteration of the same peptide in buffers containing between 10 and 90% D_2O. We found that, at a D_2O flow rate five times greater than the sample flow, a D-content of approximately 80% can be achieved (Figure 5 A), which is comparable to that conventionally used for off-line HDX [114].

We then investigated whether HDX cell deuteration accurately reflects protein folding states. For this purpose, we subjected myoglobin under native or denaturing conditions to on-line deuteration. The results indicate a significant increase in backbone labeling when denaturing conditions that increase backbone accessibility are employed (Figure 5 B), which supports the concept. We therefore concluded that global protein folding can be monitored by HDX cell deuteration.

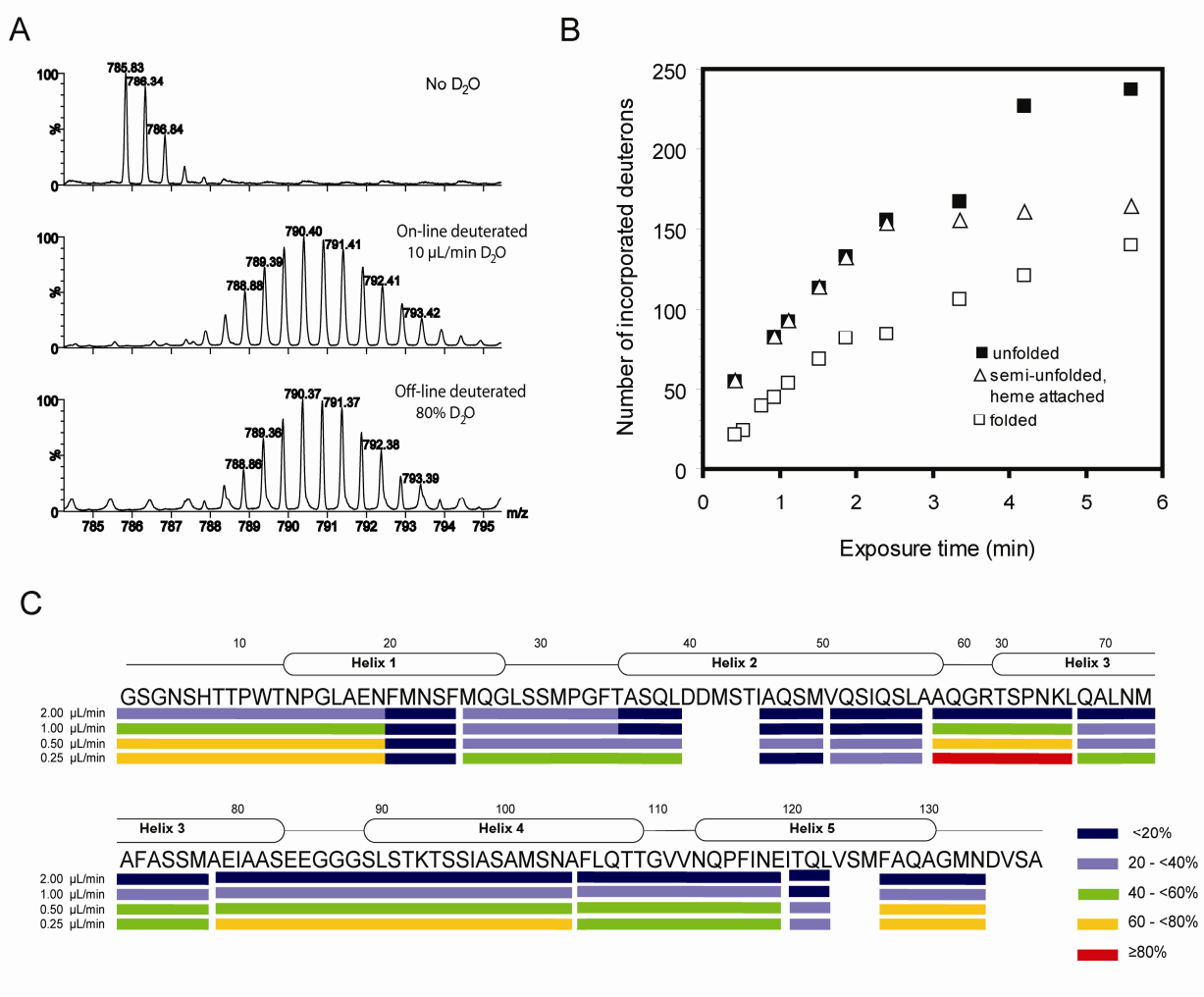

Figure 5. On-line deuteration using the HDX cell. (A) [Glu1]-fibrinopeptide B is shown as undeuterated (top), deuterated on-line in the HDX cell with a D_2O flow rate of 10 µL/min and a sample flow rate of 2 µL/min (middle), and deuterated off-line in 80% D_2O, 20% H_2O. (B) Deuteration of myoglobin at varying flow rates converted to exposure time (see Paper III for details) in H_2O (open squares) and in the presence of 35% acetonitrile without (black squares) and with heme group attached (open triangles). (C) Peptide level HDX profile of MaSp1 NT deuterated in the HDX cell at flow rates between 0.25 and 5 µL/min. Color coding indicates the degree of backbone labeling in each fragment relative to the maximum deuteration observed after off-line labeling in 80% D_2O. Adapted from Paper III.

For peptide-level HDX-MS analysis, we equipped the HDX cell setup with a pepsin column for on-line proteolytic digestion, as well as a reverse phase column for purification of the resulting peptides. On-line deuteration and digestion of the N-terminal domain of spider silk MaSp 1 resulted in a deuteration pattern that accurately reflects the presence of secondary structure elements as determined by X-ray crystallography [50] and conventional HDX-MS (Paper X) (Figure 5 C). It should be noted that protein solutions between 10 and 60 µM were employed, which is equivalent to the concentrations used during labeling reactions in conventional HDX-MS after dilution.

Taken together, our data indicate that (a) the HDX cell can achieve the D^+ concentrations necessary for effective HDX in the sample channel, and (b) HDX cell-driven HDX-MS can be used to monitor protein folding at the global and peptide levels without the need for concentrated protein stock solutions.

5 RESULTS AND DISCUSSION

5.1 CONTROL OF INSULIN AGGREGATION BY PROINSULIN C-PEPTIDE

5.1.1 C-peptide interferes with insulin fibril formation (Paper IV)

5.1.1.1 C-peptide changes the morphology of insulin amyloid-like fibrils

Firstly, we investigated the effect of C-peptide on insulin fibrillation. Incubation of insulin alone under fibril forming conditions (1 mM insulin at pH 2.5 and 75ºC) in standard microcentrifuge tubes resulted in increasing ThT fluorescence after a lag time of approximately 3 ½ h and formation of fibrillar structures visible by EM (Figure 6 A, C). Co-incubation of equimolar amounts of insulin and C-peptide under these conditions, on the other hand, resulted in significantly reduced lag time, with the appearance of ThT-postive, rounded aggregates already after 1 h (Figure 6 A and C, top panel). When incubation was carried out in Protein LoBind^{TM} tubes, which are designed to prevent protein aggregation by lack of nucleation sites, C-peptide was found to significantly extend fibrillation lag time (Figure 6 B). In both cases, EM analysis revealed that co-incubation of insulin and C-peptide resulted in the formation of clumps of short fibrils (Figure 6 C, bottom panels). Together, the data suggest that C-peptide interferes with the assembly of unfolded insulin into fibrils.

5.1.1.2 C-peptide and insulin interact during fibril formation

We concluded that these effects must be mediated by a direct molecular interaction between C-peptide and insulin. Native ESI-MS spectra during fibrillation lag phase show the presence of 1:1 complexes between insulin and C-peptide, indicating that both peptides can indeed interact under the buffer conditions employed here. MS analysis of solubilized fibrillar material confirmed the presence of both insulin and C-peptide in the aggregates. Additionally, we performed short-time deuterium labeling of insulin + C-peptide fibrils. Labeled fibrils were dissolved in formic acid and subjected to MS analysis. We observed two separate insulin populations: one with labeling behavior similar to that of fibrillated insulin, the other with additional backbone protection. This suggests the presence of two molecular conformations, which is indicative for additional structural arrangement of the insulin fibrils, or continued interactions of C-peptide with the insulin fibrils.

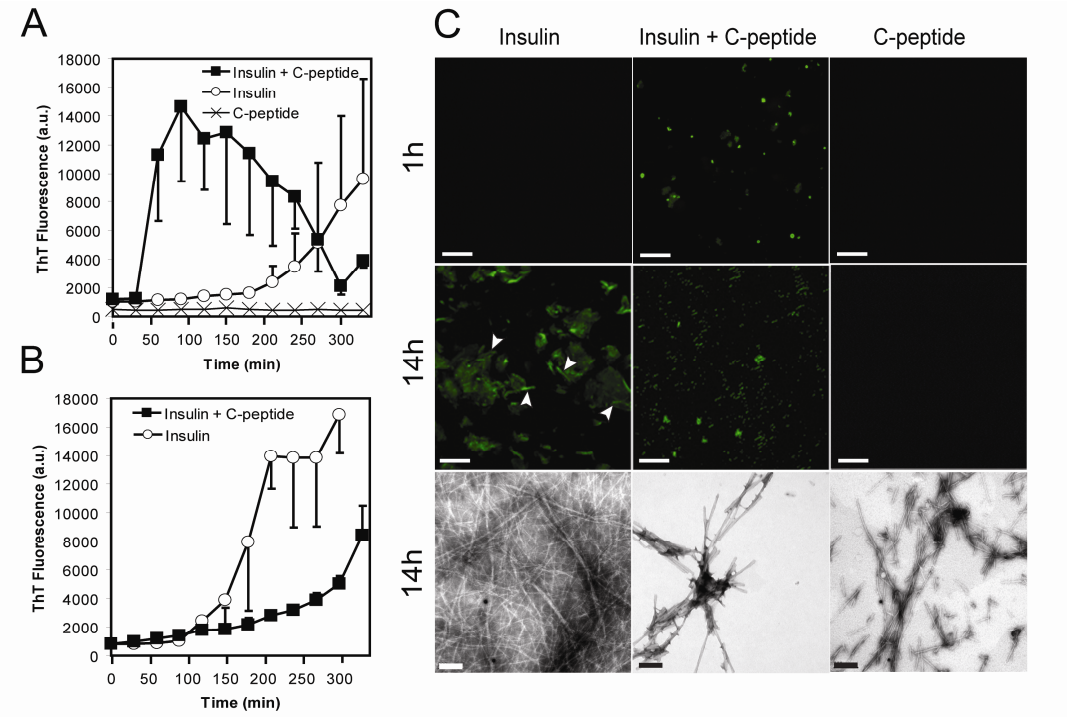

Figure 6. C-peptide interferes with insulin fibril formation. (A) ThT fluorescence time course shows acceleration of insulin fibrillation by C-peptide in regular microcentrifuge tubes. (B) Co-incubation of C-peptide and insulin in Protein LoBind™ microcentrifuge tubes delays insulin fibrillation. Error bars indicate standard deviation from four separate incubations. (C) Aggregate morphology in ThT fluorescence microscopy (top and middle row) and EM (bottom row). Co-incubation of insulin and C-peptide caused the appearance of small, round, ThT-positive aggregates after 1 h. Electron microscopy shows clumps of short, thick fibrils from co-incubation of insulin and C-peptide. Scale bars indicate 200 µM in fluorescence microscopy images and 200 nm in EM micrographs. Reproduced from Paper IV.

5.1.1.3 C-peptide as a regulator of amyloid fibril formation

Two previous studies by others have reported no effect of C-peptide on insulin fibrillation at pH 2.0 [121] and 7.3 [122]. However, both studies were conducted using low rather than high insulin concentrations (60 and 2.5 µM, respectively) in salt-containing buffers (150 and 100 mM NaCl, respectively). However, the salt concentration found in secretory exceeds that of insulin by a factor of only 5 to 10 [123], and insulin fibrils observed at the injection sites in diabetic patients are likely the result of high local insulin concentrations. Standard insulin injection solutions contain between 0.7 and 1 mM insulin and no NaCl. Since salt and insulin concentration have been described as important factors in insulin fibrillation, it is likely that use of such near-millimolar concentrations in the absence of salt cause insulin aggregation [73]. Thus, C-peptide can stabilize insulin under these conditions, opening the possibility to control insulin aggregation by an endogenous peptide.

Interestingly, the effects of C-peptide on islet amyloid polypeptide (IAPP) fibrillation are similar to those reported here. The presence of C-peptide caused significantly accelerated IAPP aggregation, leading to reduced Congo Red staining intensity and incorporation of C-peptide into fibrils with altered morphology [124, 125]. The proposed mechanism that the negatively charged C-peptide forms a stabilizing complex with the unfolded, positively charged IAPP monomer in solution, but can accelerate fibril formation if nucleation points are present, is compatible with our findings on the effect of C-peptide on insulin fibrillation. This raises the possibility of C-peptide being a general regulator of β-cell granule peptide amyloid formation (see section 5.1.3).

5.1.2 pH-dependent regulation of insulin solubility by C-peptide (Paper V)

5.1.2.1 C-peptide co-precipitates with insulin at pH 5

Having established that C-peptide affects the state of insulin under fibril-forming conditions, we asked whether C-peptide could exert a similar effect on insulin at pH values between 5 and 6, *i.e.* around the isoelectric point of insulin. Insulin processing in the secretory granules occurs at this mildly acidic pH range [126]. Its reduced solubility under these conditions is thought to drive the processed insulin into complex formation with the abundantly present zinc ions and subsequent crystallization [127]. The crystals are released into the bloodstream as long-acting insulin together with a fluid, acidic phase containing C-peptide and soluble insulin [128], suggesting that C-peptide participates in intragranular sorting [129].

Previously, we have employed native ESI-MS to monitor the effect of C-peptide on insulin oligomers observed at pH 5 that represent pre-fibrillar aggregates [63]. C-peptide removed insulin multimers from the ESI-MS spectra, which was interpreted as a desaggregating effect on insulin [61, 130]. We employed spectrophotometry and microscopy to monitor the effect of C-peptide on insulin oligomers at pH 5. Surprisingly, we observed a direct increase in the optical density at 500 nm (OD_{500}) of concentrated insulin solutions after the addition of equimolar amounts of C-peptide, indicating that the presence of C-peptide causes immediate precipitation. Isolation by centrifugation and subsequent ESI-MS analysis confirmed that the precipitate contains both C-peptide and insulin, while only C-peptide was found in the supernatant. The sub-stoichiometric incorporation of C-peptide was investigated by spectrophotometric analysis of solutions containing insulin and C-peptide at ratios between 1:1 and 1:32. Only solutions containing an insulin/C-peptide ratio of 1 or 2 were found to precipitate, which shows a strict stoichiometry of one C-peptide per two insulin moieties.

5.1.2.2 Co-precipitation is dependent on conserved C-peptide charges

To investigate whether co-precipitation provides an explanation to the observed removal of insulin oligomers from ESI-MS spectra, we repeated the ESI-MS studies with C-peptide analogues in which the conserved glutamate residues at positions 11 (E11A) or 27 (E27A) or 3, 11 and 27 (E3,11,27A) were replaced by alanines. None of the three peptides caused an increase in OD_{500} when mixed with insulin at equimolar ratios. Similarly, the presence of 100 mM NaCl inhibited co-precipitation, while increase of the pH to > 7.5 immediately dissolved the precipitate, showing that its formation depends on charged residues.

ESI-MS spectra of insulin in the presence of the E11A and E27A C-peptide variants showed only a minor reduction of insulin oligomers, while no reduction was observed the case of the E3,11,27A variant. All three variants formed heteromers with insulin oligomers at sub-stoichiometric amounts of C-peptide. CID-analysis revealed that 1:1 complexes between insulin and wt C-peptide have the same gas phase stability as those formed between insulin and the E11A or E27A variants, while insulin complexes with the E3,11,27A variant had a lower gas phase stability.

5.1.2.3 C-peptide-insulin interactions via mutual charge neutralization

Insulin has a net charge of +2 at the mildly acidic pH during secretion that was employed in this study. At the same pH, C-peptide has a net charge of -4 due to its four glutamate residues, three of which are the only largely conserved residues in the C-peptide sequence. A complex of two insulin molecules and one C-peptide would have a net charge of 0, thus lowering its solubility and causing precipitation. This is supported by evidence from gas phase interaction studies: All three C-peptide variants do not co-precipitate with insulin and cannot remove insulin oligomers from the ESI-MS spectra, but form instead non-covalent complexes. This indicates that the presence of two or three glutamate residues is sufficient for the formation of 1:1, but not 1:2 complexes with insulin. Removal of three glutamate residues, however, significantly decreases the stability of the 1:1 complex. This is compatible with wt C-peptide binding two insulin molecules together via its negative charges in a “handcuff”-like manner (Figure 7). Removal of one charge on C-peptide leaves one of the two interactions intact, while the removal of three charges weakens the remaining interaction. In all cases, the complex net charge is <0 and the complex retains its solubility.

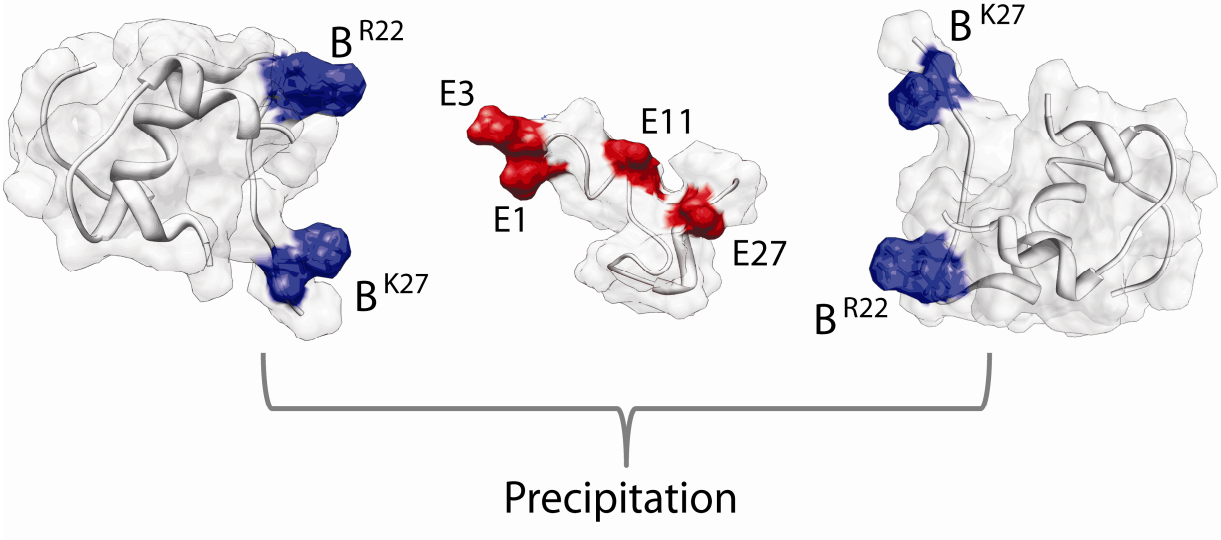

Figure 7. Proposed model for pH-dependent regulation of insulin solubility by C-peptide. At pH 5, C-peptide has a net charge of -4, while insulin has a net charge of +2. We propose a "handcuff"-like mechanism by which insulin forms a 2:1 complex with C-peptide that has a net charge of 0 and precipitates.

5.1.2.4 Implications for the prevention of insulin fibrillation in vivo

Several studies have raised the question why insulin does not form amyloid at the extreme concentration found in the secretory granules, which can exceed 20 mM [123]. It has previously been thought that zinc crystal formation catches poorly soluble processed insulin and thus prevents insulin fibrillation. However, it has been shown that zinc is not essential for production and release of biologically active insulin from pancreatic β-cell granules [131]. Additionally, the insulin released from the C-peptide-rich acidic fluid phase is biologically active, and not all granules contain zinc-insulin crystals [128].

To date, only one charge-altering C-peptide mutation has been investigated for its potential to alter insulin processing and release, and no negative effects were detected [132]. We propose a balance between zinc-mediated crystal assembly and C-peptide mediated, pH-dependent precipitation. The lowered pH following proinsulin cleavage [126] could cause protonation of insulin B-chain histidine residue 10, which is known to prevent zinc crystal formation [133]. Thus, minor pH-changes could steer insulin into crystallization or precipitation to balance the amount of long-acting and rapid-acting release forms.

5.1.3 Peptide interactions and protein aggregation in diabetes (Paper VI)

5.1.3.1 C-peptide as an aggregation inhibitor in vivo?

As described above, *in vitro* studies show that C-peptide interacts with both insulin and IAPP to prevent uncontrolled aggregation, and either type of interaction is charge-based and therefore pH-sensitive. In both cases, the effective pH range is close to that found in the secretory granules, where the peptides co-localize in the halo region.

In diabetes types 1 and 2, the synthesis and processing of granular peptides is impaired. Since insulin has an inhibitory effect on IAPP aggregation [134], it has previously been suggested that diabetes-associated disturbances in peptide synthesis and processing promote IAPP aggregation and contribute to β-cell dysfunction [135]. However, reduction in insulin processing too small to abolish the inhibitory effect on IAPP aggregation [136]. Similarly, diabetes-related changes in insulin levels do not affect the insulin:C-peptide ratio, and no insulin amyloid deposits have been found in the secretory granules. Therefore, does the finding that C-peptide can control IAPP and insulin aggregation *in vitro* have any relevance *in vivo*?

5.1.3.2 Peptide ratio imbalances may contribute to diabetes-associated protein aggregation

Even though the changes in ratios of insulin, C-peptide and IAPP as well as their respective proforms at different diabetic stages are individually too small to affect peptide aggregation, they do represent a significant deviation from normophysiology that is exacerbated as the disease progresses. In this work, we present evidence that C-peptide interacts with insulin and IAPP through the same mechanism, and therefore propose that their interactions in the secretory granules are more complex than previously thought.

In Paper V, we have proposed that a balance between charge-based co-precipitation with C-peptide and zinc-mediated crystallization contributes to intragranular insulin sorting. It has been suggested that similar charge-based interactions with C-peptide localize IAPP to the halo region [134]. Therefore, if peptide relative or absolute amounts are disturbed, such a sorting mechanism might function less efficiently or become non-functional. In this scenario, lowered amounts of C-peptide and insulin but continued high zinc content could drive insulin exclusively into crystallization. Alternatively, lowered amounts of C-peptide could be insufficient in recruiting and binding IAPP to the halo region. In both cases, IAPP would be sequestered from aggregation inhibition.

The sorting mechanism via insulin crystallization and C-peptide precipitation also offers an explanation to the fact that neither the exclusion of zinc from the secretory granule [131] nor charge-altering C-peptide mutations [132] lead to the formation of insulin aggregates. When both stabilizing components are lacking, as it is the case during administration of recombinant insulin in insulin-dependent diabetes of both types, insulin aggregates can form. In this sense, localized insulin amyloidosis can be considered an extreme case of diabetes-associated peptide imbalance.

5.2 UNRAVELLING THE ANTI-AMYLOID ACTIVITY OF BRICHOS DOMAINS

5.2.1 Binding specificity of proSP-C BRICHOS (Paper VII)

5.2.1.1 Monitoring BRICHOS-peptide interactions by ESI-MS

Based on the previously established anti-amyloid activity of CTC, we set out to determine the molecular determinants for substrate recognition by the BRICHOS domain using native ESI-MS to determine gas phase binding constants through direct titration and relative gas phase binding energies through CID. Target peptide sequences were modeled by homo-tripeptides composed of small (AAA, GGG), hydrophobic (LLL, VVV), charged (KKK) and aromatic (FFF, YYY) amino acids, all of which were amidated and acetylated to mimic longer protein segments. Additionally, we included amyloidogenic peptides (KFFE [13], $A\beta_{1-40}$) and a non-amyloidogenic β-hairpin peptide (KFFEYNGKKFFE, in the following termed "YNGK" [137]). These peptides were mixed at increasing concentrations with the purified proSP-C BRICHOS domain. Free protein [P] and the non-covalent complexes [66] were quantified directly from the spectra. The gas phase K_D was then derived by plotting the [66]/[P] ratio against the total ligand concentration [66].

We found that VVV had the lowest K_D of all tested peptides (summarized in Table 1), which fits well with the valine-rich natural target sequence of SP-C. The K_D observed for the hydrophobic aromatic peptide FFF was similarly low, while the hydrophobic peptide LLL had a much higher gas phase K_D. The highest gas phase K_D was observed for the YYY peptide, indicating that the introduction of hydroxyl groups significantly lowers binding. Interestingly, we observed a low gas phase K_D for the YNGK peptide, indicating that BRICHOS can also interact with β-hairpin peptides.

By measurement of the amount of intact protein-peptide complexes using CID with increasing collision voltages, we were able to derive relative gas phase stabilities for binding of each model peptide to the BRICHOS domain. Their order (from low to high stability) was determined to be GGG < VVV ≈ LLL ≈ KFFE ≈YNGK < FFF < YYY. Due to its greater length, $A\beta_{1-40}$ may interact with the BRICHOS domain at multiple sites and is therefore not suitable for direct comparison with shorter model peptides. We concluded that the complexes with the highest gas phase stability are formed by interaction with aromatic residues. Since it has been shown that four conserved tyrosine residues in the BRICHOS domain can be involved in ligand binding [80], it is possible that this tyrosine-rich environment can be responsible for the increased gas phase stability.

Table 1. Apparent dissociation constants (K_D) and maximum binding (B_{max}) for peptide ligands to the proSP-C Brichos domain. See Paper VII for details.

Peptide	Apparent K_D (µM)	B_{max}	R^2 [a]
AAA, KKK	- [b]	- [b]	- [b]
KFFE	- [c]	- [c]	0.710
$A\beta_{40}$	- [d]	- [d]	0.988
GGG	- [e]	- [e]	0.998
YYY	45	0.71	0.980
LLL	17	0.18	0.967
YNGK	1.7	0.11	0.996
FFF	1.4	0.27	0.928
VVV	1.2	0.07	0.979

[a] Linear correlation (0 = no correlation, 1 = perfect correlation)

[b] No quantifiable interaction observed.

[c] No interpretable titration data.

[d] K_D outside of practical titration range.

[e] Unspecific interactions.

5.2.1.2 BRICHOS gas phase and solution phase ligand preferences are comparable

To validate whether the derived gas phase ligand preferences are compatible with in-solution data, we compared the apparent K_Ds with results obtained from a membrane binding assay, where segments composed of a single amino acid were spotted on a cellulose membrane, incubated with S-tagged recombinant CTC, and subjected to immunodetection with an S-tag-reactive antibody. Subsequent quantification of the amount of CTC bound to each spot confirmed that hydrophobic and aromatic residues are the preferred binding partners of CTC [86]. Therefore, the gas phase results are comparable to those obtained under solution conditions and suggest that native ESI-MS can be utilized in the investigation of hydrophobic interactions.

5.2.2 The molecular action of the proSP-C BRICHOS domain (Paper VIII)

5.2.2.1 The high-resolution proSP-C BRICHOS structure

To map the interaction of CTC with amyloidogenic peptides at the molecular level, determination of its high-resolution crystal structure was carried out in collaboration with the group of Prof- Stefan Knight (SLU, Uppsala). After several crystallization attempts proved unsuccessful, it was found that treatment of full-length CTC with trypsin yielded material suitable for crystallization. MS analysis revealed that the crystallized protein lacked the N-terminal linker region and a shorter segment close to the C-terminus.

The crystallized protein encompassed thus residues 82-160 and 168-197 linked by two disulfide bridges and includes most of the conserved BRICHOS domain. The crystal structure determined at 2.1 Å shows a trimer. Each subunit contains a central five-stranded β-sheet enclosed by an α-helix on each side. One side of the beta sheet plane (face A) is lined with strictly conserved hydrophobic residues including the tyrosines previously suggested to be involved in peptide binding. However, access to this surface is in the crystal structure blocked by the α-helix composed of residues 134-145 (helix 1). Mapping of the conserved residues in the *SFTPC* sequence showed that the strictly conserved aspartic acid in position 105 is in contact with the C-terminal α-helix 182-190 (helix 2) and could mediate the position of both helices via non-covalent interactions. Molecular dynamics simulations carried out by Prof. Johan Åqvist and colleagues (Uppsala University) of D105Y and D105G CTC mutants resulted in partial unwinding of helix 2, which in turn moves helix 1 away from face A by 5-7 Å, thus making face A solvent accessible. It was therefore concluded that interactions via aspartic acid 105 could regulate the contact between face A and a hydrophobic ligand. This hypothesis is supported by the observation that mutations of D105 are associated with ILD in humans.

We then mapped the structure of the segments that were proteolytically removed in order to facilitate crystallization by performing HDX-MS of full-length CTC. Interestingly, no individual peptic peptides from the regions encompassing residues 110-161 and 180-197, which corresponds to the crystallized segment of CTC were observed, indicating that this region is highly protease-resistant even at pH 2. Of the segments that could be digested and subsequently analyzed by HDX-MS, the linker region (residues 67-84) and the short peptide spanning residues 161-179 acquired full deuterium labeling within 60 seconds. This indicates that the non-crystallizable segments are in fact unstructured in solution, which explains their inhibitory effect on CTC crystallization.

5.2.2.2 CTC interacts with peptide ligands via its flexible linker region

To determine whether the chaperoning effect of CTC on polyvaline target peptides can be monitored, HDX-MS of CTC was conducted in the presence of peptides containing 5 or 7 valines (V_5 and V_7) or alanines (A_7) flanked by two lysine residues at each end. Comparison of the deuteration pattern of the polyvaline peptides in the absence and the presence of CTC shows that CTC induces significant protection from exchange in a

subpopulation of ligand peptides (Figure 8). This effect is more pronounced in the longer V_7 peptide, while no additional protection is observed for the A_7 peptide.

To determine whether a distinct segment within CTC mediates this effect, we performed the same experiment with a construct encompassing only the BRICHOS domain, as well as a synthetic peptide corresponding to the linker segment only (residues 68-84). In case of the BRICHOS domain, only a minor increase in protection of the V_7 peptide could be observed, while the linker alone had no effect.

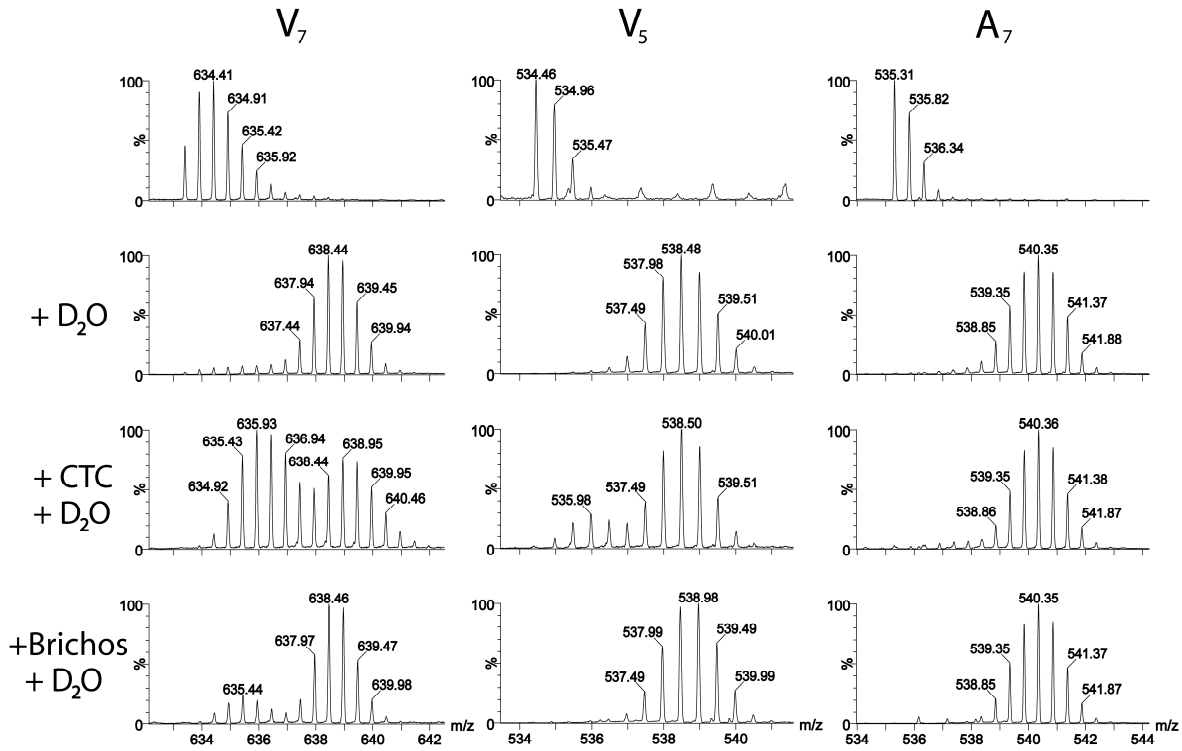

Figure 8. CTC induces increased protection from deuterium exchange in long polyvaline segments. A subpopulation of the V_7 (left column) and to a lesser extent V_5 (middle column) peptide show lower deuterium uptake in the presence of CTC. This effect is greatly reduced when only the BRICHOS domain is present. Labeling of the A_7 peptide (right column) is not influenced by CTC.

Monitoring the deuterium exchange pattern of the linker region (as the BRICHOS domain was inaccessible to peptic digestion) in the presence and the absence of the V_7 peptide showed that the N-terminal peptide encompassing residues 68-71 (VLEM) incorporates significantly less deuterium when a polyvaline segment is present (Figure 9). This indicates the induction of a secondary structure element in this region. We therefore propose a model in which the polyvaline segment is bound to face A of the BRICHOS domain in extended conformation while the linker region forms a complementary β-strand (Figure 9).

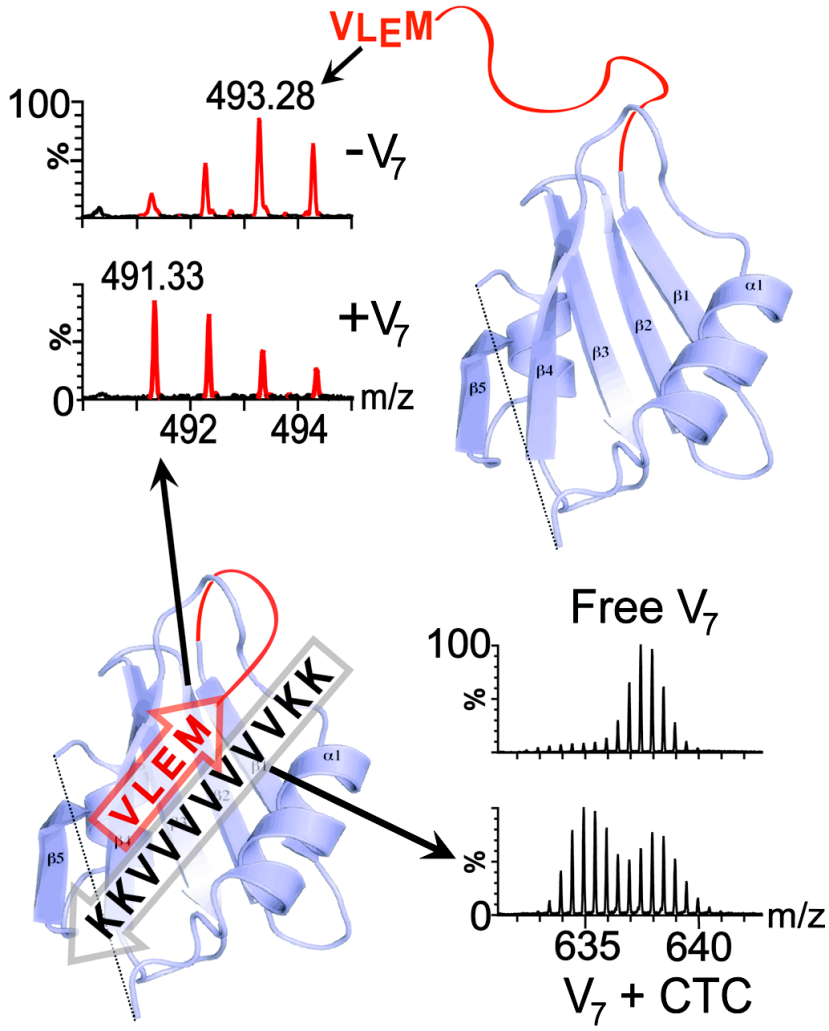

Figure 9. A schematic model of CTC action derived from HDX-MS data. A polyvaline peptide interacts with face A of the BRICHOS domain (grey arrow). The unstructured linker segment (red) forms a complementary β-strand (red arrow), which traps the amyloidogenic peptide in extended conformation and increases protection from deuterium labeling in both segments. Reproduced from Paper VIII.

5.2.2.3 CTC mutations cause amyloid formation in vivo

The importance of the linker region for the biological function of CTC is illustrated by the observation that the most prevalent mutation, in which an isoleucine in position 73 is replaced with a threonine, is located only two residues away on the C-terminal side of the VLEM fragment that is involved in peptide ligand binding (Figure 9), suggesting that the introduction of a polar amino acid in this region can interfere with the interaction of the linker with the SP-C transmembrane segment.

To investigate whether CTC malfunction can give rise to amyloid *in vivo*, the group of Prof. Per Westermark (Uppsala University) performed histological screening of lung sections obtained from seven patients with mutations in the CTC region. In all but one case, microdeposits composed of mature SP-C were observed that showed green

birefringence upon Congo Red staining when viewed under polarized light, as well as immunoreactivity of serum amyloid P component, which both are hallmarks of amyloid deposits. Therefore we concluded that CTC exerts its anti-amyloid function *in vitro* and *in vivo* via both linker and BRICHOS domain, and the ILD cases reported here an instance of an amyloid disease caused by specific chaperone dysfunction.

5.2.3 Function of the Bri2 BRICHOS domain (Paper IX)

5.2.3.1 Bri2 has anti-amyloid activity in vitro

Parallel to our studies on the BRICHOS domain structure, it was investigated whether the anti-amyloid activity observed for the proSP-C BRICHOS domain can also be exerted by the BRICHOS domain of Bri2 (ITM2B). This was carried out using a cloned and purified a construct encompassing residues 90-236 of the Bri2 protein, which includes the BRICHOS domain but not the 23-residue C-terminal peptide. The presence of the single intramolecular disulfide bond was confirmed by chemical reduction and MS.

Next, we asked if the Bri2 BRICHOS domain is able to prevent $A\beta_{1-40}$ aggregation *in vitro*. While $A\beta_{1-40}$ alone was found to aggregate within 7h, incubation of Bri2-BRICHOS with $A\beta_{1-40}$ at ratios between 1:1 and 1:10 prevented amyloid fibril formation within the 24 h period studied, as judged by ThT fluorescence. EM of solutions containing a 1:1 solution of $A\beta_{1-40}$ and Bri2 BRICHOS showed no amyloid fibrils even after 5 days of incubation at room temperature.

5.2.3.2 The Bri2 BRICHOS domain interacts with aromatic peptides

In an approach based on that presented in Paper VII, we employed ESI-MS to study interactions between Bri2-BRICHOS and its potential target peptides, the 23-residue Bri23 peptide of unkown function, and $A\beta_{1-40}$. We observed the non-covalent complexes between Bri2 BRICHOS and either peptide. However, only a minor fraction of Bri2 BRICHOS was found to interact with $A\beta_{1-40}$, while the presence of equimolar amounts of Bri23 was able to nearly completely saturate Bri2 BRICHOS. In competition between $A\beta_{1-40}$ and Bri23, $A\beta_{1-40}$ was unable to displace Bri23 from the Bri2 BRICHOS domain, indicating that the latter binds Bri23 with high affinity.

We then specified the preferred peptide ligand features by screening the homo-tripeptide library employed for proSP-C BRICHOS. Unfortunately, the Bri2 BRICHOS construct proved to be less suitable for native ESI-MS, which prevented the determination of gas phase K_Ds. However, we were able to perform qualitative binding

studies and observed that only tyrosine-containing ligands were able to interact with Bri2 BRICHOS in the gas phase. We therefore conclude that proSP-C and Bri2 BRICHOS domains have only partially overlapping ligand preferences, indicating that they possibly exert their anti-amyloid activity by targeting different regions in their ligands: While both domains are capable of interacting with peptides containing aromatic residues, which are enriched in amyloidogenic peptides [11], proSP-C BRICHOS is additionally adapted to polyvaline segments to suit its biological function.

5.3 CONTROL OF PH-DEPENDENT SPIDER SILK ASSEMBLY

5.3.1 pH-dependent action of the MaSp1 NT domain (Paper X)

5.3.1.1 MaSp1 NT dimerizes in a pH-dependent manner

To gain insights into the assembly of the MaSp1 NT domain, we recorded native ESI-MS spectra of wt and mutant NT in which conserved aspartate and glutamate residues (D40, E79, E84, and a D40E84 double mutant) are substituted for their uncharged counterparts asparagine and glutamine. Interestingly, we observed that lowering the pH from 7.0 to 6.0 resulted in a shift from mostly monomeric to dimeric wt NT protein (Figure 10), with a sharp transition between pH 6.4 and 6.3, the same pH step at which the NT domain was found to accelerate assembly of recombinant MaSp1 constructs. The D40, E84 and D40E84 mutants showed no increase in dimer formation at this pH step, while mutation of the non-conserved E79 did not affect dimerization. We therefore conclude that charge-dependent dimer formation could trigger pH-dependent assembly.

5.3.1.2 In-solution dimerization is accompanied by global fold tightening

To investigate whether the observed dimerization occurs in solution, we performed HDX-MS analysis of the NT domain at pH 6.0 and 7.0 in the presence and absence of 300 mM NaCl, and of the non-dimerizing D40E84 double mutant. Since deuterium exchange is accelerated by one order of magnitude when the pH is increased one unit [114], labeling times at pH 6.0 were extended by a factor of 10 to facilitate direct comparison of the deuterium incorporation under both conditions.

Comparison of the HDX-MS profiles at both pH values revealed a significant increase in backbone protection for helix 2 and 3, which are located at the dimer interface as determined from the crystal structure (Figure 10). This suggests that the dimerization observed by native ESI-MS occurs in solution. Interestingly, we also observed reduced deuterium uptake in peptides from the hydrophobic core of the 5-helix bundle. We interpreted this as global tightening of the NT domain, which could be a prerequisite or a result of its dimerization.

It should be noted that both conclusions -dimerization and fold tightening- were subsequently confirmed by an NMR study [138].

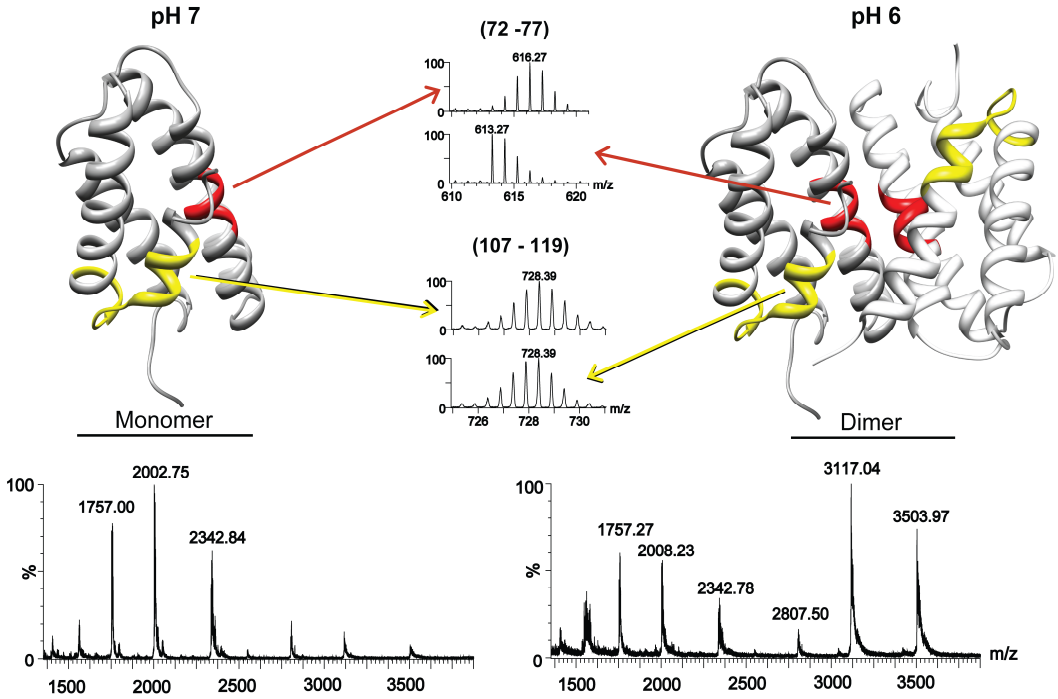

Figure 10. Monitoring structural dynamics in the MaSp1 N-terminal domain by mass spectrometry. The helical MaSp1 NT domain dimerizes when the pH is lowered from 7 (left) to 6 (right). The dimerization can be followed by an increased protection from H/D exchange in peptides located at the dimer interface as well as an increase in non-covalent dimers in ESI-MS spectra recorded at low pH. Reproduced from Paper II.

5.3.1.3 Structural changes are dependent on salt and conserved residues

The HDX-MS profiles of the D40E84 double mutant and wt NT in the presence of 300 mM NaCl showed two opposing effects. While NaCl caused globally reduced deuterium incorporation, the double mutant exhibited overall increased labeling. In both cases, however, no pH-dependent differences in deuteration could be observed, which shows that either change affects the ability of the NT domain to dimerize in a pH-dependent manner. The inhibitory effect could be mediated by shielding charged residues and forcing the protein into a more condensed structure to hide the hydrophobic core at high salt concentrations, or by global destabilization in the case of the D40E84 double mutant. Based on these data, we were able to formulate a role for the NT domain in spidroin assembly: The decrease in pH and salt during spidroin dope extrusion causes MaSp1 dimerization of the N-terminal domains. While two spidroin molecules are aligned by the parallel, covalent C-terminal domains, each NT domain links one half of this dimer to another dimer via its antiparallel dimerization ability. The arising crosslink pattern can in theory give rise to an infinite chain of MaSp1 molecules. Shear force and altered salt concentration triggers conversion of the C-terminal domain to its fiber-promoting form which initiates fiber formation.

5.3.2 The structure of monomeric MaSp1 NT (Paper XI)

5.3.2.1 The A72R NT mutant is monomeric

In order to pinpoint the structural mechanisms behind pH-dependent NT dimer formation, the structure of its monomeric form had to be determined. Since X-ray crystals structures only show the dimeric form of NT, we designed a non-dimerizing mutant, in which alanine 72, located at the center of helix 3 and extended into the dimer interface, was replaced by arginine (A72R). The positive charge and bulky side-chain of arginine should prevent dimer formation and thus facilitate study of the monomer at a wide pH range.

This was confirmed by tryptophan fluorescence spectroscopy and HDX-MS studies which show that neither the pH-dependent change in W10 fluorescence nor additional protection of helix 2 and 3 from deuteration occur in A72R at low pH. Interestingly, A72R also fails to exhibit the observed tightening of the subunit core at pH 6, suggesting that it is a result of dimer formation rather than a prerequisite.

5.3.2.2 Monomeric and dimeric NT show distinct structural differences

Structure determination of A72R by both NMR and X-ray crystallography proved successful, yielding NT structures at low and high pH. An additional NMR study of wt NT at pH 7.2 in the presence of 300 mM NaCl further confirmed that the A72R replacement did not affect the monomer structure. Therefore, a direct comparison of all structures is possible.

Under all conditions, NT retains the overall architecture of a 5-helix bundle observed in the dimer structure. However, in monomeric form, helix 1, 4 and 5 are rotated relative to helix 2 and 3, which requires the relocation of W10 from a hydrophobic crevice into a solvent-exposed conformation, thus explaining the observed differences in tryptophan fluorescence. However, no differences could be observed between the structures of A72R at pH 6 and 7, which suggests that the rotation of the helices only occurs in connection with dimerization, not as an isolated movement in connection to the pH change.

5.3.2.3 A possible mechanism for dimer formation

Since dimer formation must be regulated by conserved acidic residues, we compared their localization in monomeric and dimeric NT. In the NT dimer, the two highly

conserved residues D40 at the beginning of helix 2 and E84 at the end of helix 3 can form an intramolecular handshake interaction [50]. This interaction is lost in monomeric NT, where the two carboxylates are more than 10 Å apart, and this is accompanied by unwinding of the last half-turn of helix 3. This could be due to the lack of positive charges R60 and K65 on the opposing subunit, which are predicted to form salt bridges with the negatively charged cluster composed of residues D39, D40 and E84. ESI-MS and HDX-MS show that D40 and E84 are crucial for dimer formation, but are predicted to have a pK_a below pH 6 and are therefore unlikely to act as a pH sensor between pH 6 and 7.

To compare the structural changes upon dimerization, we constructed a hypothetical dimer composed of monomers by superimposing helices 2 and 3 in monomeric NT with the corresponding helices in each subunit in the wt NT dimer. The hypothetical dimer shows that the rotation of helix 5 causes steric clashes with helix 5 on the other subunit (Figure 11). The conserved glutamic acid residues E84 and E79 as well as the non-conserved E119 are protected from the solvent in the wt NT dimer, but become more solvent-exposed in the hypothetical dimer.

Interestingly, this is in partial agreement with molecular dynamics simulations of the wt NT dimer which predict that deprotonation of E79 and the non-conserved E119 above pH 6 allow water molecules to enter the dimer interface, causing outward rotation of helix 5, and thus destabilizing the dimer. Our data suggest that above pH 6, the repulsive charge from E79, which is predicted to have a pK_a between pH 6 and 7, prevents helix 5 from moving into the position that it occupies in the wt dimer. This is supported by ESI-MS experiments that show that the non-charged E79Q mutant is able to dimerize at both pH 7 and 6. Similarly, protonation of E119 could also reduce repulsion in this region. However, its low degree of conservation as well as the observation that replacement of E79 alone is sufficient to allow dimerization suggests that this residue is not crucial for pH-dependent dimerization.

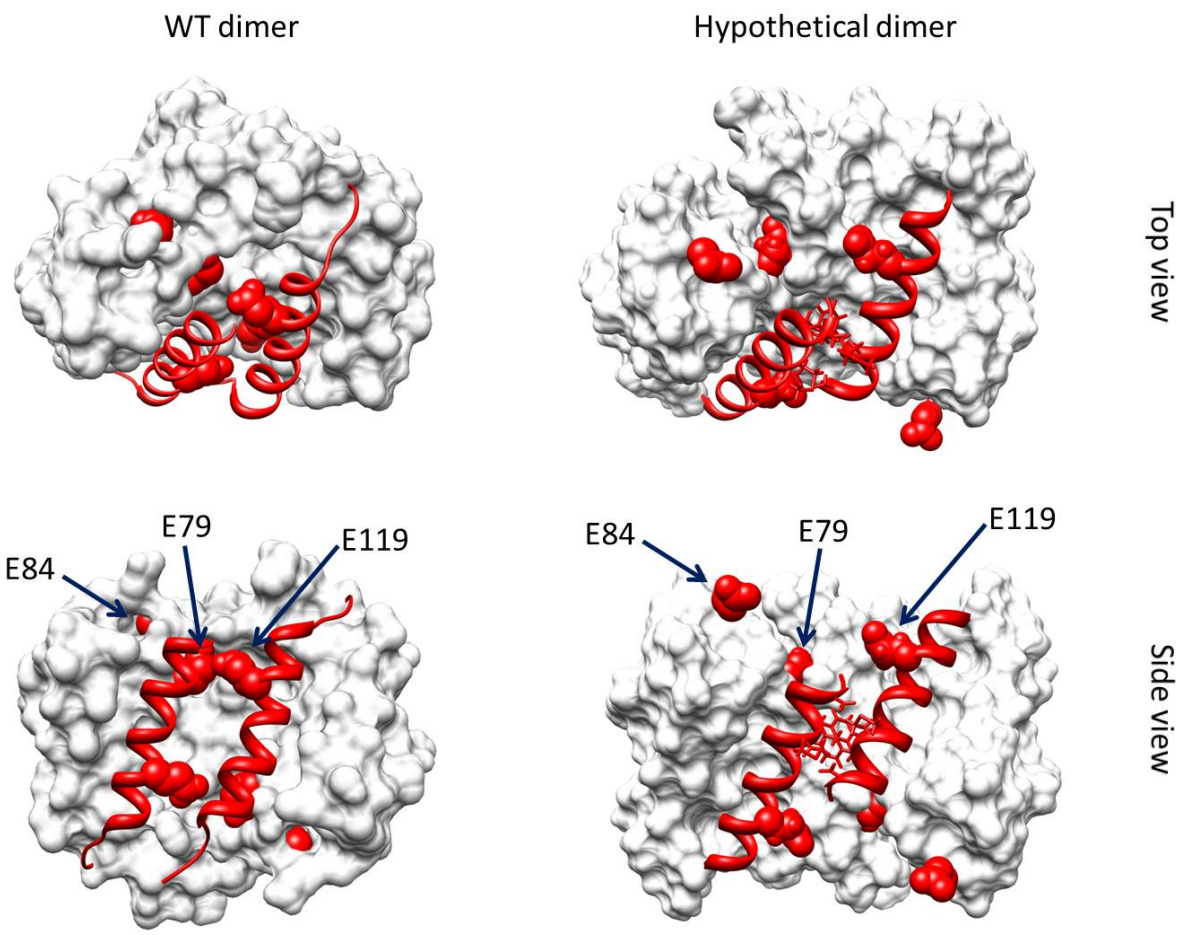

Figure 11. Dimerization of NT requires structural rearrangement of the monomer subunit and burial of glutamic acid residues. Comparison of the crystallographically determined wt NT dimer (left) and a hypothetical dimer constructed from wt monomeric NT subunits (right) as side and top view. Helix 1-4 in each dimer are shown as surface representation and helix 5 as cartoon. The side chains of E79, E84 and E119 are shown as a sphere models, clashing residues on helix 5 as stick representation. The hypothetical dimer was constructed by superimposing helices 2 and 3 in monomeric NT with the corresponding helices in each subunit in the wt NT dimer.

Together with the experimental evidence from the monomeric NT structure, conclusions about the pH-dependent dimerization mechanism can be formulated. Between pH 4 and 8, salt bridges involving the D39, D40, and E84 cluster together with R60, and K65 allow the association of two NT monomers via helix 2 and 3. However, the negative charge of E79 at pH 7 prevents helix 5 from moving into a clash-free position. At pH 6, its protonation allows the block of helix 1, 4, and 5 to rotate towards the interface and form interactions with its counterpart on the other subunit, excluding water from the interface and stabilizing the dimer (Figure 11).

5.3.3 The MaSp-1 N-terminal domain as a solubility tag (Paper XII)

5.3.3.1 MaSp1 NT as solubility-enhancing tag for protein purification

During expression and purification of recombinant NT domain variants, the wt NT domain could be easily expressed with high yields and stored at concentrations in the mM range without loss of folded, soluble protein. It appears likely that the NT domain, besides its dimerization ability, could function as a solubility tag that helps to stabilize MaSp proteins during storage in the ampullate gland.

To test this hypothesis, constructs were generated that encompassed one or two NT domains and SP-C33Leu, an SP-C variant composed of poly-leucine instead of poly-valine, which retains regular SP-C function while being less aggregation-prone . To be able to compare the efficiency of using the NT domain as solubility-enhancing tag, constructs in which SP-C33Leu was fused to the commonly used solubility tag thioredoxin (Trx) were also generated. All constructs included an N-terminal His_6-tag for affinity purification. SP-C33Leu could be released from the fusion protein by CNBr cleavage and recovery in a two-phase system of chloroform/methanol/water.

5.3.3.2 Fusion with MaSp1 NT increases protein expression and yield

While the SP-C33Leu construct tagged with Trx was expressed only at low levels, all the constructs tagged with one or two NT domains were expressed with high yield. The construct encompassing two NT domains was recovered from the soluble fraction of the bacterial lysate, while the fusion protein with a single NT domain could be purified from the membrane fraction with the addition of the detergent. This indicates that the hydrophobic SP-C33Leu is inserted into the bacterial membranes when fused to a single NT domain, and thus anchors the entire construct to the lipid fraction. The use of a single Trx tag alone, on the other hand, does not provide enough solubility.

To test whether intact SP-C33Leu can be released from the purified fusion protein, we subjected the CNBr-cleaved SP-C33Leu to ESI-MS analysis and sequencing by CID. Spectra of SP-C33Leu in 100% ethanol show pure SP-C33Leu with four or three charges, as well as a dimeric form with seven charges (Figure 12 A). CID of the $[M+3H]^{3+}$ peak confirmed that full-length SP-C33Leu had been recovered (Figure 12 B). Together, the data show that the NT domain can be used as potent solubility tag in the purification of hydrophobic peptides that are difficult to express and purify using conventional strategies. Furthermore, the data support the possibility that this feature of the NT domain could be part of its function *in vivo* by increasing the solubility of MaSp 1 to facilitate storage in the ampullate gland.

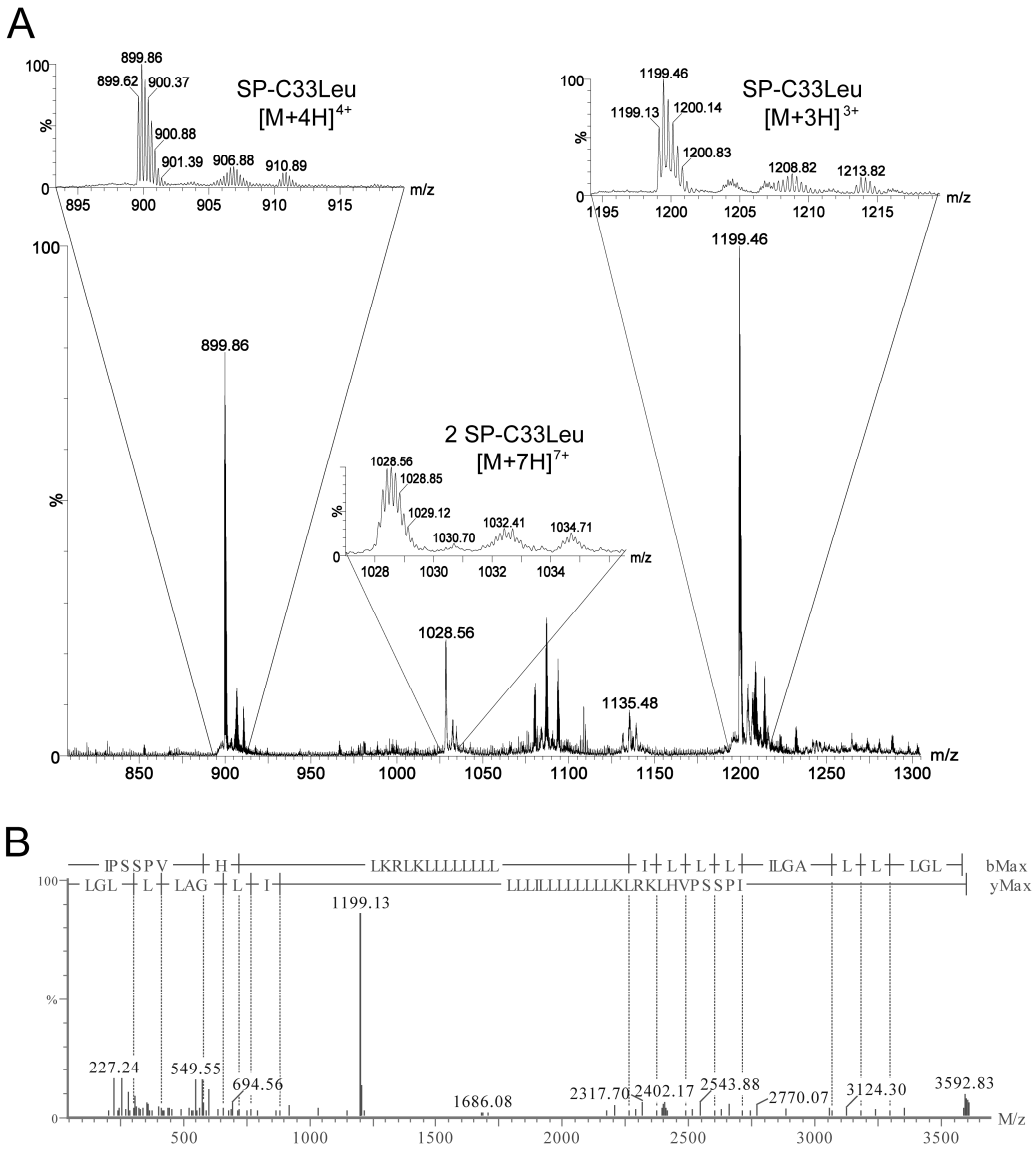

Figure 12. Characterization of SP-C33Leu recovered from NT domain fusion proteins. (A) ESI-MS shows the presence of CNBr-cleaved SP-C33Leu. (B) CID of the $[M+3H]^{3+}$ peak confirms the presence of full-length SP-C33Leu. Reproduced from Paper XII.

6 CONCLUSIONS AND OUTLOOK (PAPER XIII)

In this thesis, we have presented insights into the control of amyloid formation by autoregulatory elements in amyloidogenic (pro)proteins at the molecular level. This thesis proposes that C-peptide modulates insulin solubility via direct molecular interactions that can interfere with amyloid fibril formation, establishes that trapping an amyloidogenic segment in a β-hairpin conformation by the BRICHOS chaperone domain prevents the aggregation of SP-C, and demonstrates that dimerization of a solubility-conferring domain mediates pH-dependent assembly of spider silk.

At the time of writing, three additional systems have been described in which amyloid formation is controlled by distinct autoregulatory elements. The N-terminal side of the yeast HET-s prion co-aggregates during amyloid formation by HET-S protein, which causes refolding of its C-terminal domain. This terminates fibril extension and thus controls non-genetic heredity in yeast [139]. The fungal surface modifier protein EAS can contain or release its amyloidogenic segment based on exposure to an air:water interface [140]. The human melanin synthesis scaffold protein Pmel17 contains glutamic acid residues that allow self-association only at the acidic pH found in melanosomes [141].

Additionally, two functional amyloid systems are suggested to employ autoregulatory strategies: The Drosophila CPEB homolog Orb2a contains a short 8-residue segment that changes the amyloid formation propensity of its glutamine-rich prion domain and thus initiates the formation of amyloid-like oligomers in Drosophila mushroom body neurons that facilitate long-term memory [142], and storage of peptide hormones has been suggested to occur in amyloid form, with currently undetermined aggregation and resolubilization steps [48].

The involvement of amyloid in such highly complex systems suggests a special role for its regulation in biology and leaves much to be investigated. Even within the limited scope of this thesis, several questions remain unanswered, as summarized below.

1. We propose a mechanism by which intravesicular pH controls a balance of C-peptide- and zinc-mediated insulin phase transitions. This implies that a possible reason this mechanism has gone unnoticed is the requirement for a double mutation to generate a loss-of-function phenotype. For the biogenesis of C-peptide-related neonatal diabetes (*i.e.* impaired secretion of functional insulin

due to genetic causes), the ZnT8 transporter required for Zinc homeostasis in the secretory granules would have to be impaired [131] and one or more conserved glutamate residues in C-peptide must also be mutated. Additionally, previous studies have suggested that C-peptide glutamate residues are important for insulin folding [60]. This makes it difficult to attribute any effects of C-peptide mutations on the secretion of biologically active insulin to a specific misfolding mechanism. On the other hand, as demonstrated in Paper VIII, the detection of amyloid microdeposits requires targeted and meticulous investigations, and it is not impossible that C-peptide-related insulin aggregation has in fact gone unnoticed. Therefore, further studies on the subject are needed.

2. The high β-sheet propensity of SP-C can easily be abolished by exchange of its valine residues for leucines. Yet, evolutionary pressure has apparently not corrected this “design flaw”. Our results obtained from the proSP-C and Bri2 BRICHOS domains propose that it might be more advantageous to develop a protein domain with anti-amyloid activity that can be installed in different functional settings instead of tuning the aggregation propensity in each amyloidogenic protein individually. However, whether BRICHOS domains really have a general anti-amyloid function similar to the proposed “amyloid scavenger” protease insulin degrading enzyme [143] remains to be investigated.
3. The assembly-controlling functions of spider silk protein C- and N-terminal domains show that the secondary structure of a stretch of >3000 residues can be controlled by two <130 residue-domains. It has been proposed that storage of MaSp proteins occurs in “micelle” form, with the folded terminal domains function analogous to the polar head groups in lipid micelles [138]. However, no direct evidence for this model has been presented yet. Therefore, our understanding of the assembly of spider silk from the soluble dope is incomplete until the structural arrangements of spidroins in the ampullate gland storage form has been described in more detail.

The above points represent new points of departure in the journey towards understanding the biology of amyloid. Personally, I am positive that eventually answers to these and the many other remaining questions will hold the key to a targeted, efficient approach for tackling amyloid disease. This is the reason we conduct our investigations.

7 ACKNOWLEDGEMENTS

First of all, I am deeply indebted to my three main supervisors, **Hans Jörnvall, Janne Johansson,** and **Tomas Bergman.** You were the driving force of this operation and have worked together effortlessly so that I was supported by not one, but THREE times the dedication, experience, and inspiration, and I have learned much from all of you!

Tomas, you were my first contact in the lab and took the risk of accepting me as PhD student. Your vast knowledge, kind personality and talent both as a scientist and a teacher have been an important support for me. You made all of this possible in the first place!
Hans, you set up my PhD project by bringing people and ideas together, and you have chosen me as the last student in your long and successful career, which I feel is a great honor. I can't thank you enough.
Janne, you said yes to this project without hesitation and made me a part of your exciting research. You and your entire group have a fantastic energy, and it is always a real treat for me when I am able to contribute. I really enjoy working with you and I think we really "click".

My co-supervisor **Krister Kristensson**: You were always there with a great attitude and lots of enthusiasm! Thanks for the introduction to prion work I got from you and Elin, and I look forward to continuing our work!

Lars Tjernberg: Thank you for being my mentor! Even if I never had any issues to bring to you, you were always welcoming and ready to listen and help (and, besides that, providing excellent amyloid expertise at the drop of a dime)!

The grand old classic **HEJ-Lab** and all who were in it:
The MBB boy group: Andreas, Frank and Linus, fan vad kul det är med er! Essam "Dr. E" Refai who is the kindest man on earth! The humble and yet humbling Prof. Janne Sjövall: you are not only a legend and a walking treasure chest of knowledge, you have done very much for me, and I will always be indebted to you! Our guardian angel Ingegerd Nylander. Prof. Jan-Olof Höög, Prof. Birgitta Agerberth and her amazing group: Erica Miraglia, Monika Lind, Protim Sarker, Ylva Kai-Larsen, Rokeya Sultana

Rekha, Åke “HoHoHo!” Nordberg, and Peter Bergman. Juan Astorga-Wells especially for his endless supply of ideas, the really, really wonderful Claudia Staab-Weijnitz, Charlotte Nerelius (big hug!), Jawed Shafqat and Emma Lindahl, who are the original C-peptide people, Mikko Hellgren, Karl Bodin, Theres Jägerbrink, Susanne Vollmer-Kasab, and of course the incredible Timo Gemoll!
And an extra-big THANK YOU to the **PAC lab**, who saved me more than once from crashing into a ditch: Gunvor Alvelius, Ella Cederlund, Carina Palmberg and Marie Ståhlberg! You are great!!

The (past and present) **JJ-Lab** members:
Kerstin Nordling, without whose incredible abilities much of this thesis would not exist! Jenny Presto, Hanna Willander, Anna Rising and My Hedhammar: thank you for your support, ideas, and reliability! Eric, Ronnie, Anton, Mona, Sara, Siwei, Urmi and Stefan, even if I wasn’t at your place all that often, you always made me feel right at home when I walked in! Thank you!

My co-authors in other places:
The **SLU crystallographers**: Gelareh “The Hurricane” Askarieh: we are synergy!! And of course Prof. Stefan D. Knight (“What’s with the name change? A pseudonym?”).
The **KI-KS Pediatric Endocrinology lab**: Prof. Olle Söder, der werte Herr Doktor Jan-Bernd “Schmierig!” Stukenborg and the entire testis group: Keep the balls rolling!
The **Madrid Surfactant lab**: Prof. Cristina Casals and her group for sending emails that are like gift-wrapped packets full of beautiful data!
Prof. **Per Westermark** and the Uppsala amyloid group: You truly bridge the gap between bench and clinic, and that is very inspiring to see!

The many, many **colleagues** at MBB and beyond, Doreen, Bernie, Jason, Olle-Bulle, Jodie, Magnus, Dominik, Åke, Susanne, Agneta, Roman, David “Better than” Good, Doro, Ássmundur, Olle R., Alessandra, the very patient Carlos, and of course the Swedish Society for Mass Spectrometry and Waters Corp. for inviting me as speaker to their meetings!

I would also like to extend a very special thanks to my **previous teachers**:
Gerd Burgbacher (Veterinäruntersuchungsamt Krefeld) for telling me there is such a thing as mass spec,
Astrid and Andrew Benie (now Novo Nordisk, Copenhagen), for their wonderful friendship, and Thomas Peters (Uni Lübeck) for opening his lab and giving me the best start possible,
Hans van Leeuwen (Uni Leiden) and Jolanda Liefhebber (now MRC Glasgow) for the many lections in lab work plus the massive amount of fun we had,
The amazing Nancy Bonini (UPenn) and Nan Liu (now UCSD) (who are so bright I have to wear shades when talking to them!), for the huge amount of support and freedom that was plain unthinkable for a little intern like me.

Alla **mina vänner** som gör livet bra varje dag: Rita und Ida, Emma & David, Frida, Petter och Uma, Julia, Fredrik och Dexter, Sarah, Reginald, Teres och Teo, Dominik och Maria, the ever-so-stylish Shazhad, Marie och Adam, Dr. Susi, Arnika und Thore, Michael, Achim, Albert, Antje, Martin und Eva, Anders och Felicia, and of course Min! Group hug!!

Danke meinen lieben **Eltern** und **Georg & Anja** und **Alex & Annika** für so viel, das kann man hier gar nicht aufzählen.

Der grösste Dank aber geht an **Luise** und **Jonathan**, meine Augensterne, dafür dass es Euch gibt. <3

8 REFERENCES

1. Kyle, R. A. (2011) Amyloidosis: a brief history, *Amyloid.* **18 Suppl 1**, 1-2.

2. Sipe, J. D. & Cohen, A. S. (2000) Review: history of the amyloid fibril, *J Struct Biol.* **130**, 88-98.

3. Greenwald, J. & Riek, R. (2010) Biology of amyloid: structure, function, and regulation, *Structure.* **18**, 1244-60.

4. Wasmer, C., Lange, A., Van Melckebeke, H., Siemer, A. B., Riek, R. & Meier, B. H. (2008) Amyloid fibrils of the HET-s(218-289) prion form a beta solenoid with a triangular hydrophobic core, *Science.* **319**, 1523-6.

5. Sawaya, M. R., Sambashivan, S., Nelson, R., Ivanova, M. I., Sievers, S. A., Apostol, M. I., Thompson, M. J., Balbirnie, M., Wiltzius, J. J., McFarlane, H. T., Madsen, A. O., Riekel, C. & Eisenberg, D. (2007) Atomic structures of amyloid cross-beta spines reveal varied steric zippers, *Nature.* **447**, 453-7.

6. Goldschmidt, L., Teng, P. K., Riek, R. & Eisenberg, D. (2009) Identifying the amylome, proteins capable of forming amyloid-like fibrils, *Proc Natl Acad Sci U S A.* **107**, 3487-92.

7. Fändrich, M., Fletcher, M. A. & Dobson, C. M. (2001) Amyloid fibrils from muscle myoglobin, *Nature.* **410**, 165-6.

8. Nelson, R., Sawaya, M. R., Balbirnie, M., Madsen, A. O., Riekel, C., Grothe, R. & Eisenberg, D. (2005) Structure of the cross-beta spine of amyloid-like fibrils, *Nature.* **435**, 773-8.

9. Nelson, R. & Eisenberg, D. (2006) Recent atomic models of amyloid fibril structure, *Curr Opin Struct Biol.* **16**, 260-5.

10. Makin, O. S., Atkins, E., Sikorski, P., Johansson, J. & Serpell, L. C. (2005) Molecular basis for amyloid fibril formation and stability, *Proc Natl Acad Sci U S A.* **102**, 315-20.

11. Gazit, E. (2005) Mechanisms of amyloid fibril self-assembly and inhibition. Model short peptides as a key research tool, *FEBS J.* **272**, 5971-8.

12. Gazit, E. (2002) A possible role for pi-stacking in the self-assembly of amyloid fibrils, *FASEB J.* **16**, 77-83.

13. Tjernberg, L., Hosia, W., Bark, N., Thyberg, J. & Johansson, J. (2002) Charge attraction and beta propensity are necessary for amyloid fibril formation from tetrapeptides, *J Biol Chem.* **277**, 43243-6.

14. Lopez de la Paz, M. & Serrano, L. (2004) Sequence determinants of amyloid fibril formation, *Proc Natl Acad Sci U S A.* **101**, 87-92.

15. Lopez de la Paz, M., Lacroix, E., Ramirez-Alvarado, M. & Serrano, L. (2001) Computer-aided design of beta-sheet peptides, *J Mol Biol.* **312**, 229-46.

16. Deechongkit, S., Powers, E. T., You, S. L. & Kelly, J. W. (2005) Controlling the morphology of cross beta-sheet assemblies by rational design, *J Am Chem Soc.* **127**, 8562-70.

17. Pawar, A. P., Dubay, K. F., Zurdo, J., Chiti, F., Vendruscolo, M. & Dobson, C. M. (2005) Prediction of "aggregation-prone" and "aggregation-susceptible" regions in proteins associated with neurodegenerative diseases, *J Mol Biol.* **350**, 379-92.

18. Kallberg, Y., Gustafsson, M., Persson, B., Thyberg, J. & Johansson, J. (2001) Prediction of amyloid fibril-forming proteins, *J Biol Chem.* **276**, 12945-50.

19. Johansson, J., Szyperski, T., Curstedt, T. & Wüthrich, K. (1994) The NMR structure of the pulmonary surfactant-associated polypeptide SP-C in an apolar solvent contains a valyl-rich alpha-helix, *Biochemistry.* **33**, 6015-23.

20. Szyperski, T., Vandenbussche, G., Curstedt, T., Ruysschaert, J. M., Wuthrich, K. & Johansson, J. (1998) Pulmonary surfactant-associated polypeptide C in a mixed organic solvent transforms from a monomeric alpha-helical state into insoluble beta-sheet aggregates, *Protein Sci.* **7**, 2533-40.

21. Hijirida, D. H., Do, K. G., Michal, C., Wong, S., Zax, D. & Jelinski, L. W. (1996) 13C NMR of Nephila clavipes major ampullate silk gland, *Biophys J.* **71**, 3442-7.

22. van Beek, J. D., Hess, S., Vollrath, F. & Meier, B. H. (2002) The molecular structure of spider dragline silk: folding and orientation of the protein backbone, *Proc Natl Acad Sci U S A.* **99**, 10266-71.

23. Simmons, A. H., Michal, C. A. & Jelinski, L. W. (1996) Molecular orientation and two-component nature of the crystalline fraction of spider dragline silk, *Science.* **271**, 84-7.

24. Slotta, U., Hess, S., Spiess, K., Stromer, T., Serpell, L. & Scheibel, T. (2007) Spider silk and amyloid fibrils: a structural comparison, *Macromol Biosci.* **7**, 183-8.

25. Sipe, J. D., Benson, M. D., Buxbaum, J. N., Ikeda, S., Merlini, G., Saraiva, M. J. & Westermark, P. (2010) Amyloid fibril protein nomenclature: 2010 recommendations from the nomenclature committee of the International Society of Amyloidosis, *Amyloid.* **17**, 101-4.

26. Vidal, R., Revesz, T., Rostagno, A., Kim, E., Holton, J. L., Bek, T., Bojsen-Moller, M., Braendgaard, H., Plant, G., Ghiso, J. & Frangione, B. (2000) A decamer duplication in the 3' region of the BRI gene originates an amyloid peptide that is associated with dementia in a Danish kindred, *Proc Natl Acad Sci U S A.* **97**, 4920-5.

27. Vidal, R., Frangione, B., Rostagno, A., Mead, S., Revesz, T., Plant, G. & Ghiso, J. (1999) A stop-codon mutation in the BRI gene associated with familial British dementia, *Nature.* **399**, 776-81.

28. Prusiner, S. B. (1982) Novel proteinaceous infectious particles cause scrapie, *Science.* **216**, 136-44.

29. Eisele, Y. S., Obermüller, U., Heilbronner, G., Baumann, F., Kaeser, S. A., Wolburg, H., Walker, L. C., Staufenbiel, M., Heikenwalder, M. & Jucker, M. (2010) Peripherally applied Abeta-containing inoculates induce cerebral beta-amyloidosis, *Science.* **330**, 980-2.

30. Dische, F. E., Wernstedt, C., Westermark, G. T., Westermark, P., Pepys, M. B., Rennie, J. A., Gilbey, S. G. & Watkins, P. J. (1988) Insulin as an amyloid-fibril protein at sites of repeated insulin injections in a diabetic patient, *Diabetologia.* **31**, 158-61.

31. Vincent, I. J. & Davies, P. (1992) A protein kinase associated with paired helical filaments in Alzheimer disease, *Proc Natl Acad Sci U S A.* **89**, 2878-82.

32. Scherzinger, E., Lurz, R., Turmaine, M., Mangiarini, L., Hollenbach, B., Hasenbank, R., Bates, G. P., Davies, S. W., Lehrach, H. & Wanker, E. E. (1997) Huntingtin-encoded polyglutamine expansions form amyloid-like protein aggregates in vitro and in vivo, *Cell.* **90**, 549-58.

33. Ueda, K., Fukushima, H., Masliah, E., Xia, Y., Iwai, A., Yoshimoto, M., Otero, D. A., Kondo, J., Ihara, Y. & Saitoh, T. (1993) Molecular cloning of cDNA encoding an unrecognized component of amyloid in Alzheimer disease, *Proc Natl Acad Sci U S A.* **90**, 11282-6.

34. Magrane, J., Smith, R. C., Walsh, K. & Querfurth, H. W. (2004) Heat shock protein 70 participates in the neuroprotective response to intracellularly expressed beta-amyloid in neurons, *J Neurosci.* **24**, 1700-6.

35. Klucken, J., Shin, Y., Masliah, E., Hyman, B. T. & McLean, P. J. (2004) Hsp70 Reduces alpha-Synuclein Aggregation and Toxicity, *J Biol Chem.* **279**, 25497-502.

36. Auluck, P. K., Chan, H. Y., Trojanowski, J. Q., Lee, V. M. & Bonini, N. M. (2002) Chaperone suppression of alpha-synuclein toxicity in a Drosophila model for Parkinson's disease, *Science.* **295**, 865-8.

37. Chan, H. Y., Warrick, J. M., Gray-Board, G. L., Paulson, H. L. & Bonini, N. M. (2000) Mechanisms of chaperone suppression of polyglutamine disease: selectivity, synergy and modulation of protein solubility in Drosophila, *Hum Mol Genet.* **9**, 2811-20.

38. Warrick, J. M., Chan, H. Y., Gray-Board, G. L., Chai, Y., Paulson, H. L. & Bonini, N. M. (1999) Suppression of polyglutamine-mediated neurodegeneration in Drosophila by the molecular chaperone HSP70, *Nat Genet.* **23**, 425-8.

39. Cohen, E., Bieschke, J., Perciavalle, R. M., Kelly, J. W. & Dillin, A. (2006) Opposing activities protect against age-onset proteotoxicity, *Science.* **313**, 1604-10.

40. Kieran, D., Kalmar, B., Dick, J. R., Riddoch-Contreras, J., Burnstock, G. & Greensmith, L. (2004) Treatment with arimoclomol, a coinducer of heat shock proteins, delays disease progression in ALS mice, *Nat Med.* **10**, 402-5.

41. Muchowski, P. J. & Wacker, J. L. (2005) Modulation of neurodegeneration by molecular chaperones, *Nat Rev Neurosci.* **6**, 11-22.

42. Olsen, A., Jonsson, A. & Normark, S. (1989) Fibronectin binding mediated by a novel class of surface organelles on Escherichia coli, *Nature.* **338**, 652-5.

43. Chapman, M. R., Robinson, L. S., Pinkner, J. S., Roth, R., Heuser, J., Hammar, M., Normark, S. & Hultgren, S. J. (2002) Role of Escherichia coli curli operons in directing amyloid fiber formation, *Science.* **295**, 851-5.

44. Claessen, D., Rink, R., de Jong, W., Siebring, J., de Vreugd, P., Boersma, F. G., Dijkhuizen, L. & Wosten, H. A. (2003) A novel class of secreted hydrophobic proteins is involved in aerial hyphae formation in Streptomyces coelicolor by forming amyloid-like fibrils, *Genes Dev.* **17**, 1714-26.

45. Otzen, D. & Nielsen, P. H. (2008) We find them here, we find them there: functional bacterial amyloid, *Cell Mol Life Sci.* **65**, 910-27.

46. Shorter, J. & Lindquist, S. (2005) Prions as adaptive conduits of memory and inheritance, *Nat Rev Genet.* **6**, 435-50.

47. Fowler, D. M., Koulov, A. V., Alory-Jost, C., Marks, M. S., Balch, W. E. & Kelly, J. W. (2006) Functional amyloid formation within mammalian tissue, *PLoS Biol.* **4**, e6.

48. Maji, S. K., Perrin, M. H., Sawaya, M. R., Jessberger, S., Vadodaria, K., Rissman, R. A., Singru, P. S., Nilsson, K. P., Simon, R., Schubert, D., Eisenberg, D., Rivier, J., Sawchenko, P., Vale, W. & Riek, R. (2009) Functional amyloids as natural storage of peptide hormones in pituitary secretory granules, *Science.* **325**, 328-32.

49. Shorter, J. & Lindquist, S. (2004) Hsp104 catalyzes formation and elimination of self-replicating Sup35 prion conformers, *Science.* **304**, 1793-7.

50. Askarieh, G., Hedhammar, M., Nordling, K., Saenz, A., Casals, C., Rising, A., Johansson, J. & Knight, S. D. (2010) Self-assembly of spider silk proteins is controlled by a pH-sensitive relay *Nature.* **465**, 236-238.

51. Blundell, T. L., Cutfield, J. F., Cutfield, S. M., Dodson, E. J., Dodson, G. G., Hodgkin, D. C., Mercola, D. A. & Vijayan, M. (1971) Atomic positions in rhombohedral 2-zinc insulin crystals, *Nature.* **231**, 506-11.

52. Steiner, D. F., Cunningham, D., Spigelman, L. & Aten, B. (1967) Insulin biosynthesis: evidence for a precursor, *Science.* **157**, 697-700.

53. Lindahl, E., Nyman, U., Melles, E., Sigmundsson, K., Stahlberg, M., Wahren, J., Obrink, B., Shafqat, J., Joseph, B. & Jörnvall, H. (2007) Cellular internalization of proinsulin C-peptide, *Cell Mol Life Sci.* **64**, 479-86.

54. Lindahl, E., Nyman, U., Zaman, F., Palmberg, C., Cascante, A., Shafqat, J., Takigawa, M., Savendahl, L., Jörnvall, H. & Joseph, B. (2009) Proinsulin C-peptide regulates ribosomal RNA expression, *J Biol Chem.* **285**, 3462-9.

55. Rigler, R., Pramanik, A., Jonasson, P., Kratz, G., Jansson, O. T., Nygren, P., Stahl, S., Ekberg, K., Johansson, B., Uhlen, S., Uhlen, M., Jörnvall, H. & Wahren, J. (1999) Specific binding of proinsulin C-peptide to human cell membranes, *Proc Natl Acad Sci U S A.* **96**, 13318-23.

56. Munte, C. E., Vilela, L., Kalbitzer, H. R. & Garratt, R. C. (2005) Solution structure of human proinsulin C-peptide, *FEBS J.* **272**, 4284-93.

57. Lind, J., Lindahl, E., Peralvarez-Marin, A., Holmlund, A., Jörnvall, H. & Mäler, L. (2010) Structural features of proinsulin C-peptide oligomeric and amyloid states, *FEBS J.* **277**, 3759-68.

58. Qiao, Z. S., Min, C. Y., Hua, Q. X., Weiss, M. A. & Feng, Y. M. (2003) In vitro refolding of human proinsulin. Kinetic intermediates, putative disulfide-forming pathway folding initiation site, and potential role of C-peptide in folding process, *J Biol Chem.* **278**, 17800-9.

59. Min, C. Y., Qiao, Z. S. & Feng, Y. M. (2004) Unfolding of human proinsulin. Intermediates and possible role of its C-peptide in folding/unfolding, *Eur J Biochem.* **271**, 1737-47.

60. Chen, L. M., Yang, X. W. & Tang, J. G. (2002) Acidic residues on the N-terminus of proinsulin C-Peptide are important for the folding of insulin precursor, *J Biochem.* **131**, 855-9.

61. Shafqat, J., Melles, E., Sigmundsson, K., Johansson, B. L., Ekberg, K., Alvelius, G., Henriksson, M., Johansson, J., Wahren, J. & Jörnvall, H. (2006) Proinsulin C-peptide elicits disaggregation of insulin resulting in enhanced physiological insulin effects, *Cell Mol Life Sci.* **63**, 1805-11.

62. Jörnvall, H., Lindahl, E., Astorga-Wells, J., Lind, J., Holmlund, A., Melles, E., Alvelius, G., Nerelius, C., Maler, L. & Johansson, J. (2010) Oligomerization and insulin interactions of proinsulin C-peptide: Threefold relationships to properties of insulin, *Biochem Biophys Res Commun.* **391**, 1561-6.

63. Nettleton, E. J., Tito, P., Sunde, M., Bouchard, M., Dobson, C. M. & Robinson, C. V. (2000) Characterization of the oligomeric states of insulin in self-assembly and amyloid fibril formation by mass spectrometry, *Biophys J.* **79**, 1053-65.

64. Tito, P., Nettleton, E. J. & Robinson, C. V. (2000) Dissecting the hydrogen exchange properties of insulin under amyloid fibril forming conditions: a site-specific investigation by mass spectrometry, *J Mol Biol.* **303**, 267-78.

65. Hua, Q. X. & Weiss, M. A. (2004) Mechanism of insulin fibrillation: the structure of insulin under amyloidogenic conditions resembles a protein-folding intermediate, *J Biol Chem.* **279**, 21449-60.

66. Ahmad, A., Uversky, V. N., Hong, D. & Fink, A. L. (2005) Early events in the fibrillation of monomeric insulin, *J Biol Chem.* **280**, 42669-75.

67. Jimenez, J. L., Nettleton, E. J., Bouchard, M., Robinson, C. V., Dobson, C. M. & Saibil, H. R. (2002) The protofilament structure of insulin amyloid fibrils, *Proc Natl Acad Sci U S A.* **99**, 9196-201.

68. Swift, B. (2002) Examination of insulin injection sites: an unexpected finding of localized amyloidosis, *Diabet Med.* **19**, 881-2.

69. Yumlu, S., Barany, R., Eriksson, M. & Rocken, C. (2009) Localized insulin-derived amyloidosis in patients with diabetes mellitus: a case report, *Hum Pathol.* **40**, 1655-60.

70. Ludwig, D. B., Webb, J. N., Fernandez, C., Carpenter, J. F. & Randolph, T. W. (2011) Quaternary conformational stability: The effect of reversible self-association on the fibrillation of two insulin analogs, *Biotechnol Bioeng*.

71. Nagaveni, V., Sravani, M., Prabhakar, S., Sreedhar, B. & Vairamani, M. (2011) Targeting insulin amyloid assembly by aminosugars and their derivatives, *Protein Pept Lett.* **18**, 588-93.

72. Devlin, G. L., Knowles, T. P., Squires, A., McCammon, M. G., Gras, S. L., Nilsson, M. R., Robinson, C. V., Dobson, C. M. & MacPhee, C. E. (2006) The component polypeptide chains of bovine insulin nucleate or inhibit aggregation of the parent protein in a conformation-dependent manner, *J Mol Biol.* **360**, 497-509.

73. Brange, J., Andersen, L., Laursen, E. D., Meyn, G. & Rasmussen, E. (1997) Toward understanding insulin fibrillation, *J Pharm Sci.* **86**, 517-25.

74. Levy-Sakin, M., Shreberk, M., Daniel, Y. & Gazit, E. (2009) Targeting insulin amyloid assembly by small aromatic molecules: toward rational design of aggregation inhibitors, *Islets.* **1**, 210-5.

75. Arora, A., Ha, C. & Park, C. B. (2004) Inhibition of insulin amyloid formation by small stress molecules, *FEBS Lett.* **564**, 121-5.

76. Gibson, T. J. & Murphy, R. M. (2006) Inhibition of insulin fibrillogenesis with targeted peptides, *Protein Sci.* **15**, 1133-41.

77. Sanchez-Pulido, L., Devos, D. & Valencia, A. (2002) BRICHOS: a conserved domain in proteins associated with dementia, respiratory distress and cancer, *Trends Biochem Sci.* **27**, 329-32.

78. Hayami, T., Shukunami, C., Mitsui, K., Endo, N., Tokunaga, K., Kondo, J., Takahashi, H. E. & Hiraki, Y. (1999) Specific loss of chondromodulin-I gene expression in chondrosarcoma and the suppression of tumor angiogenesis and growth by its recombinant protein in vivo, *FEBS Lett.* **458**, 436-40.

79. Hedlund, J., Johansson, J. & Persson, B. (2009) BRICHOS - a superfamily of multidomain proteins with diverse functions, *BMC Res Notes.* **2**, 180.

80. Casals, C., Johansson, H., Saenz, A., Gustafsson, M., Alfonso, C., Nordling, K. & Johansson, J. (2008) C-terminal, endoplasmic reticulum-lumenal domain of prosurfactant protein C - structural features and membrane interactions, *FEBS J.* **275**, 536-47.

81. Willander, H., Hermansson, E., Johansson, J. & Presto, J. (2011) BRICHOS domain associated with lung fibrosis. dementia and cancer - a chaperone that prevents amyloid fibril formation?, *FEBS J.* **278,** 3893-904.

82. Nerelius, C., Martin, E., Peng, S., Gustafsson, M., Nordling, K., Weaver, T. & Johansson, J. (2008) Mutations linked to interstitial lung disease can abrogate anti-amyloid function of prosurfactant protein C, *Biochem J.* **416**, 201-9.

83. Brasch, F., Griese, M., Tredano, M., Johnen, G., Ochs, M., Rieger, C., Mulugeta, S., Muller, K. M., Bahuau, M. & Beers, M. F. (2004) Interstitial lung disease in a baby with a de novo mutation in the SFTPC gene, *Eur Respir J.* **24**, 30-9.

84. Tredano, M., Griese, M., Brasch, F., Schumacher, S., de Blic, J., Marque, S., Houdayer, C., Elion, J., Couderc, R. & Bahuau, M. (2004) Mutation of SFTPC in infantile pulmonary alveolar proteinosis with or without fibrosing lung disease, *Am J Med Genet A.* **126A**, 18-26.

85. Johansson, H., Eriksson, M., Nordling, K., Presto, J. & Johansson, J. (2009) The Brichos domain of prosurfactant protein C can hold and fold a transmembrane segment, *Protein Sci.* **18**, 1175-82.

86. Johansson, H., Nerelius, C., Nordling, K. & Johansson, J. (2009) Preventing amyloid formation by catching unfolded transmembrane segments, *J Mol Biol.* **389**, 227-9.

87. Akiyama, H., Kondo, H., Arai, T., Ikeda, K., Kato, M., Iseki, E., Schwab, C. & McGeer, P. L. (2004) Expression of BRI, the normal precursor of the amyloid protein of familial British dementia, in human brain, *Acta Neuropathol.* **107**, 53-8.

88. Kim, S. H., Wang, R., Gordon, D. J., Bass, J., Steiner, D. F., Lynn, D. G., Thinakaran, G., Meredith, S. C. & Sisodia, S. S. (1999) Furin mediates enhanced production of fibrillogenic ABri peptides in familial British dementia, *Nat Neurosci.* **2**, 984-8.

89. Fotinopoulou, A., Tsachaki, M., Vlavaki, M., Poulopoulos, A., Rostagno, A., Frangione, B., Ghiso, J. & Efthimiopoulos, S. (2005) BRI2 interacts with amyloid precursor protein (APP) and regulates amyloid beta (Abeta) production, *J Biol Chem.* **280**, 30768-72.

90. Kim, J., Miller, V. M., Levites, Y., West, K. J., Zwizinski, C. W., Moore, B. D., Troendle, F. J., Bann, M., Verbeeck, C., Price, R. W., Smithson, L., Sonoda, L., Wagg, K., Rangachari, V., Zou, F., Younkin, S. G., Graff-Radford, N., Dickson, D., Rosenberry, T. & Golde, T. E. (2008) BRI2 (ITM2b) inhibits Abeta deposition in vivo, *J Neurosci.* **28**, 6030-6.

91. Matsuda, S., Tamayev, R. & D'Adamio, L. (2011) Increased AbetaPP Processing in Familial Danish Dementia Patients, *J Alzheimers Dis*. **27,** 385-91.

92. Matsuda, S., Matsuda, Y., Snapp, E. L. & D'Adamio, L. (2009) Maturation of BRI2 generates a specific inhibitor that reduces APP processing at the plasma membrane and in endocytic vesicles, *Neurobiol Aging.* **32**, 1400-8.

93. Li, X., Eles, P. T. & Michal, C. A. (2009) Water permeability of spider dragline silk, *Biomacromolecules.* **10**, 1270-5.

94. Cetinkaya, M., Xiao, S., Markert, B., Stacklies, W. & Grater, F. (2011) Silk fiber mechanics from multiscale force distribution analysis, *Biophys J.* **100**, 1298-305.

95. Vollrath, F. & Knight, D. P. (1999) Structure and function of the silk production pathway in the spider Nephila edulis, *Int J Biol Macromol.* **24**, 243-9.

96. Dicko, C., Vollrath, F. & Kenney, J. M. (2004) Spider silk protein refolding is controlled by changing pH, *Biomacromolecules.* **5**, 704-10.

97. Knight, D. P. & Vollrath, F. (2001) Changes in element composition along the spinning duct in a Nephila spider, *Naturwissenschaften.* **88**, 179-82.

98. Chen, X., Knight, D. P. & Vollrath, F. (2002) Rheological characterization of nephila spidroin solution, *Biomacromolecules.* **3**, 644-8.

99. Ayoub, N. A., Garb, J. E., Tinghitella, R. M., Collin, M. A. & Hayashi, C. Y. (2007) Blueprint for a high-performance biomaterial: full-length spider dragline silk genes, *PLoS ONE.* **2**, e514.

100. Hayashi, C. Y., Shipley, N. H. & Lewis, R. V. (1999) Hypotheses that correlate the sequence, structure, and mechanical properties of spider silk proteins, *Int J Biol Macromol.* **24**, 271-5.

101. Stark, M., Grip, S., Rising, A., Hedhammar, M., Engström, W., Hjalm, G. & Johansson, J. (2007) Macroscopic fibers self-assembled from recombinant miniature spider silk proteins, *Biomacromolecules.* **8**, 1695-701.

102. Ittah, S., Cohen, S., Garty, S., Cohn, D. & Gat, U. (2006) An essential role for the C-terminal domain of a dragline spider silk protein in directing fiber formation, *Biomacromolecules.* **7**, 1790-5.

103. Huemmerich, D., Scheibel, T., Vollrath, F., Cohen, S., Gat, U. & Ittah, S. (2004) Novel assembly properties of recombinant spider dragline silk proteins, *Curr Biol.* **14**, 2070-4.

104. Hagn, F., Eisoldt, L., Hardy, J. G., Vendrely, C., Coles, M., Scheibel, T. & Kessler, H. (2010) A conserved spider silk domain acts as a molecular switch that controls fibre assembly, *Nature.* **465**, 239-42.

105. Rising, A., Widhe, M., Johansson, J. & Hedhammar, M. (2010) Spider silk proteins: recent advances in recombinant production, structure-function relationships and biomedical applications, *Cell Mol Life Sci.* **68**, 169-84.

106. Ganem, B., Li, Y.-T. & Henion, J. D. (1991) Detection of non-covalent receptor-ligand complexes by mass spectrometry, *J Am Chem Soc.* **113**, 6294-6296.

107. Breuker, K. & McLafferty, F. W. (2008) Stepwise evolution of protein native structure with electrospray into the gas phase, 10(-12) to 10(2) s, *Proc Natl Acad Sci U S A.* **105**, 18145-52.

108. Breuker, K., Bruschweiler, S. & Tollinger, M. (2010) Electrostatic stabilization of a native protein structure in the gas phase, *Angew Chem Int Ed Engl.* **50**, 873-7.

109. Loo, J. A. (1997) Studying noncovalent protein complexes by electrospray ionization mass spectrometry, *Mass Spectrom Rev.* **16**, 1-23.

110. Veros, C. T. & Oldham, N. J. (2007) Quantitative determination of lysozyme-ligand binding in the solution and gas phases by electrospray ionisation mass spectrometry, *Rapid Commun Mass Spectrom.* **21**, 3505-10.

111. Ruotolo, B. T., Giles, K., Campuzano, I., Sandercock, A. M., Bateman, R. H. & Robinson, C. V. (2005) Evidence for macromolecular protein rings in the absence of bulk water, *Science.* **310**, 1658-61.

112. Englander, S. W., Mayne, L., Bai, Y. & Sosnick, T. R. (1997) Hydrogen exchange: the modern legacy of Linderstrom-Lang, *Protein Sci.* **6**, 1101-9.

113. Englander, S. W. (2006) Hydrogen exchange and mass spectrometry: A historical perspective, *J Am Soc Mass Spectrom.* **17**, 1481-9.

114. Morgan, C. R. & Engen, J. R. (2009) Investigating solution-phase protein structure and dynamics by hydrogen exchange mass spectrometry, *Curr Protoc Protein Sci.* Chapter **17**, Unit 17 6 1-17.

115. Katta, V. & Chait, B. T. (1991) Conformational changes in proteins probed by hydrogen-exchange electrospray-ionization mass spectrometry, *Rapid Commun Mass Spectrom.* **5**, 214-7.

116. Zhang, Z. & Smith, D. L. (1993) Determination of amide hydrogen exchange by mass spectrometry: a new tool for protein structure elucidation, *Protein Sci.* **2**, 522-31.

117. Kheterpal, I., Zhou, S., Cook, K. D. & Wetzel, R. (2000) Abeta amyloid fibrils possess a core structure highly resistant to hydrogen exchange, *Proc Natl Acad Sci U S A.* **97**, 13597-601.

118. Kheterpal, I., Williams, A., Murphy, C., Bledsoe, B. & Wetzel, R. (2001) Structural features of the Abeta amyloid fibril elucidated by limited proteolysis, *Biochemistry.* **40**, 11757-67.

119. Lu, X., Wintrode, P. L. & Surewicz, W. K. (2007) Beta-sheet core of human prion protein amyloid fibrils as determined by hydrogen/deuterium exchange, *Proc Natl Acad Sci U S A.* **104**, 1510-5.

120. Smirnovas, V., Baron, G. S., Offerdahl, D. K., Raymond, G. J., Caughey, B. & Surewicz, W. K. (2011) Structural organization of brain-derived mammalian prions examined by hydrogen-deuterium exchange, *Nat Struct Mol Biol.* **18**, 504-6.

121. Huang, K., Dong, J., Phillips, N. B., Carey, P. R. & Weiss, M. A. (2005) Proinsulin is refractory to protein fibrillation: topological protection of a precursor protein from cross-beta assembly, *J Biol Chem.* **280**, 42345-55.

122. Noormagi, A., Gavrilova, J., Smirnova, J., Tougu, V. & Palumaa, P. Zn(II) ions co-secreted with insulin suppress inherent amyloidogenic properties of monomeric insulin, *Biochem J.* **430**, 511-8.

123. Foster, M. C., Leapman, R. D., Li, M. X. & Atwater, I. (1993) Elemental composition of secretory granules in pancreatic islets of Langerhans, *Biophys J.* **64**, 525-32.

124. Westermark, G., Arora, M. B., Fox, N., Carroll, R., Chan, S. J., Westermark, P. & Steiner, D. F. (1995) Amyloid formation in response to beta cell stress occurs in vitro, but not in vivo, in islets of transgenic mice expressing human islet amyloid polypeptide, *Mol Med.* **1**, 542-53.

125. Janciauskiene, S., Eriksson, S., Carlemalm, E. & Ahren, B. (1997) B cell granule peptides affect human islet amyloid polypeptide (IAPP) fibril formation in vitro, *Biochem Biophys Res Commun.* **236**, 580-5.

126. Orci, L., Ravazzola, M., Amherdt, M., Madsen, O., Perrelet, A., Vassalli, J. D. & Anderson, R. G. (1986) Conversion of proinsulin to insulin occurs coordinately with acidification of maturing secretory vesicles, *J Cell Biol.* **103**, 2273-81.

127. Steiner, D. F. (1973) Cocrystallization of proinsulin and insulin, *Nature.* **243**, 528-30.

128. Michael, D. J., Ritzel, R. A., Haataja, L. & Chow, R. H. (2006) Pancreatic beta-cells secrete insulin in fast- and slow-release forms, *Diabetes.* **55**, 600-7.

129. Steiner, D. F. (2004) The proinsulin C-peptide--a multirole model, *Exp Diabesity Res.* **5**, 7-14.

130. Nerelius, C., Alvelius, G. & Jörnvall, H. (2010) N-terminal segment of proinsulin C-peptide active in insulin interaction/desaggregation, *Biochem Biophys Res Commun.* **403**, 462-7.

131. Lemaire, K., Ravier, M. A., Schraenen, A., Creemers, J. W., Van de Plas, R., Granvik, M., Van Lommel, L., Waelkens, E., Chimienti, F., Rutter, G. A., Gilon, P., in't Veld, P. A. & Schuit, F. C. (2009) Insulin crystallization depends on zinc transporter ZnT8 expression, but is not required for normal glucose homeostasis in mice, *Proc Natl Acad Sci U S A.* **106**, 14872-7.

132. Park, S. Y., Ye, H., Steiner, D. F. & Bell, G. I. (2011) Mutant proinsulin proteins associated with neonatal diabetes are retained in the endoplasmic reticulum and not efficiently secreted, *Biochem Biophys Res Commun.* **391**, 1449-54.

133. Ishikawa, T., Chatake, T., Morimoto, Y., Maeda, M., Kurihara, K., Tanaka, I. & Niimura, N. (2008) An abnormal pK(a) value of internal histidine of the insulin molecule revealed by neutron crystallographic analysis, *Biochem Biophys Res Commun.* **376**, 32-5.

134. Westermark, P., Li, Z. C., Westermark, G. T., Leckström, A. & Steiner, D. F. (1996) Effects of beta cell granule components on human islet amyloid polypeptide fibril formation, *FEBS Lett.* **379**, 203-6.

135. Hayden, M. R., Tyagi, S. C., Kerklo, M. M. & Nicolls, M. R. (2005) Type 2 diabetes mellitus as a conformational disease, *J Pancr.* **6**, 287-302.

136. Larson, J. L. & Miranker, A. D. (2004) The mechanism of insulin action on islet amyloid polypeptide fiber formation, *J Mol Biol.* **335**, 221-31.

137. Hosia, W., Bark, N., Liepinsh, E., Tjernberg, A., Persson, B., Hallen, D., Thyberg, J., Johansson, J. & Tjernberg, L. (2004) Folding into a beta-hairpin can prevent amyloid fibril formation, *Biochemistry.* **43**, 4655-61.

138. Hagn, F., Thamm, C., Scheibel, T. & Kessler, H. (2011) pH-dependent dimerization and salt-dependent stabilization of the N-terminal domain of spider dragline silk--implications for fiber formation, *Angew Chem Int Ed Engl.* **50**, 310-3.

139. Greenwald, J., Buhtz, C., Ritter, C., Kwiatkowski, W., Choe, S., Maddelein, M. L., Ness, F., Cescau, S., Soragni, A., Leitz, D., Saupe, S. J. & Riek, R. (2010) The mechanism of prion inhibition by HET-S, *Mol Cell.* **38**, 889-99.

140. Macindoe, I., Kwan, A. H., Ren, Q., Morris, V. K., Yang, W., Mackay, J. P. & Sunde, M. (2012) Self-assembly of functional, amphipathic amyloid monolayers by the fungal hydrophobin EAS, *Proc Natl Acad Sci U S A*. **109,** 804-11.

141. Pfefferkorn, C. M., McGlinchey, R. P. & Lee, J. C. (2010) Effects of pH on aggregation kinetics of the repeat domain of a functional amyloid, Pmel17, *Proc Natl Acad Sci U S A.* **107**, 21447-52.

142. Majumdar, A., Cesario, W. C., White-Grindley, E., Jiang, H., Ren, F., Khan, M. R., Li, L., Choi, E. M., Kannan, K., Guo, F., Unruh, J., Slaughter, B. & Si, K. (2012) Critical Role of Amyloid-like Oligomers of Drosophila Orb2 in the Persistence of Memory, *Cell*.

143. Kurochkin, I. V. (2001) Insulin-degrading enzyme: embarking on amyloid destruction, *Trends Biochem Sci.* **26**, 421-5.